



24 **ABSTRACT**

25 Sleep is a nearly universal feature of animal behaviour, yet many of the molecular, genetic,  
26 and neuronal substrates that orchestrate sleep/wake transitions lie undiscovered. Employing a  
27 viral insertion sleep screen in larval zebrafish, we identified a novel gene, *dreammist* (*dmist*),  
28 whose loss results in behavioural hyperactivity and reduced sleep at night. The neuronally  
29 expressed *dmist* gene is conserved across vertebrates and encodes a small single-pass  
30 transmembrane protein that is structurally similar to the Na<sup>+</sup>,K<sup>+</sup>-ATPase regulator,  
31 FXD1/Phospholemman. Disruption of either *fxd1* or *atp1a3a*, a Na<sup>+</sup>,K<sup>+</sup>-ATPase alpha-3  
32 subunit associated with several heritable movement disorders in humans, led to decreased  
33 night-time sleep. Since *atp1a3a* and *dmist* mutants have elevated intracellular Na<sup>+</sup> levels and  
34 non-additive effects on sleep amount at night, we propose that Dmist-dependent enhancement  
35 of Na<sup>+</sup> pump function modulates neuronal excitability to maintain normal sleep behaviour.

36

37 **INTRODUCTION**

38 The ability of animals to switch between behaviourally alert and quiescent states is  
39 conserved across the animal kingdom (Cirelli, 2009; Joiner, 2016). Fundamental processes  
40 that govern the regulation of sleep-like states are shared across species, such as the roles of  
41 circadian and homeostatic cues in regulating the time and amount of sleep, stereotyped  
42 postures, heightened arousal thresholds, and the rapid reversibility to a more alert state (Joiner,  
43 2016). The near ubiquity of sleep implies that it serves ancient functions and is subject to  
44 conserved regulatory processes. However, many key molecular components that modulate  
45 sleep and wake states remain undiscovered.

46 Over the past two decades, investigations into sleep and arousal states of genetically  
47 tractable model organisms, such as *Drosophila melanogaster*, *C. elegans*, and *Danio rerio*  
48 (zebrafish) have uncovered novel molecular and neuronal components of sleep regulation

49 through gain- and loss-of-function genetic screens (reviewed in Barlow and Rihel, 2017; Sehgal  
50 and Mignot, 2011). The power of screening approaches is perhaps best exemplified by the first  
51 forward genetic sleep screen, which identified the potassium channel *shaker* as a critical sleep  
52 regulator in *Drosophila* (Cirelli et al., 2005). This result continues to have a lasting impact on  
53 the field, as not only did subsequent sleep screening efforts uncover the novel Shaker regulator  
54 *sleepless*, (Koh et al., 2009), but investigations into Shaker's beta subunit Hyperkinetic  
55 ultimately revealed a critical role for this redox sensor linking metabolic function to sleep  
56 (Bushey et al., 2007; Kempf et al., 2019).

57 Disparate screening strategies across model organisms continue to unveil novel sleep  
58 modulators in both invertebrate and vertebrate model systems. For example, the roles of  
59 RFamide receptor DMSR-1 in stress-induced sleep in *C. elegans* (Iannacone et al., 2017) and  
60 SIK3 kinase in modulating sleep homeostasis in mice (Funato et al., 2016) were identified in  
61 genetic screens. Moreover, a gain of function screening strategy in *Drosophila* revealed the  
62 novel sleep and immune regulator, *nemuri* (Toda et al., 2019), and a zebrafish overexpression  
63 screen uncovered the secreted neuropeptides neuromedin U and neuropeptide Y, which  
64 decrease and increase sleep, respectively (Chiu et al., 2016; Singh et al., 2017). The success  
65 of screening strategies in revealing novel sleep-wake regulatory genes suggests that more  
66 sleep signals likely remain to be discovered.

67 One of the lessons from these genetic screens is that many of the uncovered genes play  
68 conserved roles across species. For example, Shaker also regulates mammalian sleep  
69 (Douglas et al., 2007) and RFamides induce sleep in worms, flies, and vertebrates (Lee et al.,  
70 2017; Lenz et al., 2015). Nevertheless, not every invertebrate sleep-regulatory gene has a  
71 clear vertebrate homolog, while some human sleep/wake regulators, such as the narcolepsy-  
72 associated neuropeptide hypocretin/orexin (Chemelli et al., 1999; Lin et al., 1999; Peyron et  
73 al., 2000; Sakurai, 2013), lack invertebrate orthologs. Therefore, genetic sleep screens in

74 vertebrates are likely to provide added value in uncovering additional regulatory components  
75 required to control the initiation and amount of sleep in humans.

76 While sleep screening in mammals is feasible (Funato et al., 2016), it remains an expensive  
77 and technically challenging endeavour. With its genetic tractability, availability of high-  
78 throughput sleep assays (Rihel and Schier, 2013), and conserved sleep genetics, such as the  
79 hypocretin, melatonin, locus coeruleus, and raphe systems (Gandhi et al., 2015; Singh et al.,  
80 2015; Oikonomou et al., 2019; Prober et al., 2006), the larval zebrafish is an attractive  
81 vertebrate system for sleep screens. We took advantage of a collection of zebrafish lines that  
82 harbour viral-insertions in >3500 genes (Varshney et al., 2013) to perform a targeted genetic  
83 screen. We identified a short-sleeping mutant, *dreammist*, with a disrupted novel, highly  
84 conserved vertebrate gene that encodes a small single pass transmembrane protein.  
85 Sequence and structural homology to the Na<sup>+</sup>/K<sup>+</sup> pump regulator FXYD1/Phospholemman  
86 suggests that Dreammist is a neuronal-expressed member of a class of sodium pump  
87 modulators that is important for regulating sleep-wake behaviour.



## 88 RESULTS

### 89 Reverse genetic screen identifies *dreammist*, a mutant with decreased sleep

90 We used the 'Zenemark' viral-insertion based zebrafish gene knock-out resource (Varshney  
91 et al., 2013) to perform a reverse genetic screen to identify novel vertebrate sleep genes. This  
92 screening strategy offers several advantages compared to traditional chemical mutagenesis-  
93 based forward genetic screening approaches. First, unlike chemical mutagenesis, which  
94 introduces mutations randomly, viral insertions tend to target the 5' end of genes, typically  
95 causing genetic loss of function (Sivasubbu et al., 2007). Second, because the virus sequence  
96 is known, it is straightforward to map and identify the causative gene in mutant animals. Finally,  
97 since viral insertions in the Zenemark collection are already mapped and sequenced, animals  
98 harbouring insertions within specific gene classes can be selected for testing (Figure S1A).  
99 This allowed us to prioritise screening of genes encoding protein classes that are often linked  
100 to behaviour, such as G-protein coupled receptors, neuropeptide ligands, ion channels, and  
101 transporters (Supplemental Data 1).

102 For screening, we identified zebrafish sperm samples from the Zenemark collection  
103 (Varshney et al., 2013) that harboured viral insertions in genes of interest and used these  
104 samples for *in vitro* fertilization and the establishment of F2 families, which we were able to  
105 obtain for 26 lines. For each viral insertion line, clutches from heterozygous F2 in-crosses were  
106 raised to 5 days post-fertilisation (dpf) and tracked using videography (Figure S1A) to quantify  
107 the number and duration of sleep bouts (defined in zebrafish larvae as inactivity lasting 1  
108 minute or longer; Prober et al., 2006) and waking activity (time spent moving per active bout)  
109 over 48 hours. The genotypes of individual larvae were determined by PCR after behavioural  
110 tracking, with each larva assigned as wild type, heterozygous, or homozygous for a given viral  
111 insertion to assess the effect of genotype on sleep/wake behaviour. While most screened  
112 heterozygous and homozygous lines had minimal effects on sleep-wake behavioural

113 parameters (Figure S1B-S1C), one homozygous viral insertion line, *10543/10543*, had a  
114 reduction in daytime sleep (Figure S1B) and an increase in daytime waking activity (Figure  
115 S1C) relative to their wild type sibling controls. We re-named this *10543* viral insertion line  
116 *dreammist* (*dmist*).

117 In follow-up studies, we observed that animals homozygous for the viral insertion at this  
118 locus (*dmist<sup>vir/vir</sup>*) showed a decrease in sleep during the day and a trend to sleep less at night  
119 compared to their wild-type siblings (*dmist<sup>+/+</sup>*) (Figure 1A). *dmist* mutants had an almost 50%  
120 reduction in the average amount of daytime sleep (Figure 1C) due to a decrease in the number  
121 of sleep bouts (Figure 1D), whereas the sleep bout length at night was significantly reduced  
122 (Figure 1E). *dmist<sup>vir/vir</sup>* larvae also exhibited significantly increased daytime waking activity,  
123 which is the locomotor activity while awake (Figure 1B, 1F). Because Zenemark lines can  
124 contain more than one viral insertion (17.6% of lines have  $\geq 2$  insertions; Varshney et al 2013),  
125 we outcrossed *dmist<sup>vir/+</sup>* fish to wild-type fish of the AB-TL background and re-tested *dmist*  
126 mutant fish over several generations. Normalising all the behavioural parameters to *dmist<sup>+/+</sup>*  
127 controls with a linear mixed effects (LME) model showed consistent sleep changes in *dmist<sup>vir/vir</sup>*  
128 fish over 5 independent experiments (Figure 1G). The *dmist<sup>vir/vir</sup>* larvae consistently show a  
129 more than 50% decrease in sleep during the day due to a significant reduction in the number  
130 and duration of sleep bouts, as well as a large increase in waking activity (Figure 1G). The  
131 *dmist<sup>vir/vir</sup>* mutants also had a significant reduction in sleep at night compared to wild type  
132 siblings (Figure 1G). These effects on sleep and wakefulness are not due to alterations in  
133 circadian rhythms, as behavioural period length in fish that were entrained and then shifted to  
134 free-running constant dark conditions was unaffected in *dmist<sup>vir/vir</sup>* compared to wild-type sibling  
135 larvae (Figure S2A-S2C).

136

137 **The *dmist* gene encodes a novel, small transmembrane protein**

138 Having identified a sleep mutant, we next sought to investigate the target gene disrupted by  
139 the viral insertion. Line 10543 (*dmist<sup>vir</sup>*) was initially selected for screening due to a predicted  
140 disruption of a gene encoding a serotonin transporter (*slc6a4b*) on chromosome 5. However,  
141 mapping of the *dmist* viral insertion site by inverse-PCR and sequencing revealed that the virus  
142 was instead inserted into the intron of a small two-exon gene annotated in the Zv6 genome  
143 assembly as a long intergenic non-coding RNA (lincRNA; gene transcript  
144 ENSDART00000148146, gene name *si:dkey234h16.7*), which lies approximately 6 kilobases  
145 (kb) downstream of the *slc6a4b* gene in zebrafish. At least part of this region is syntenic across  
146 vertebrates, with a small two-exon gene identified adjacent to the genes *ankrd13a* and *GIT* in  
147 several vertebrates, including human and mouse (Figure 2A). Amplifying both 5' and 3' ends  
148 of zebrafish *si:dkey234h16.7* and mouse E13.5 1500011B03-001 transcripts with Rapid  
149 Amplification of cDNA ends (RACE) confirmed the annotated zebrafish and mouse transcripts  
150 and identified two variants with 3' untranslated regions (3'UTR) of different lengths in zebrafish  
151 (Figure S3B). To test whether the viral insertion in *dmist<sup>vir/vir</sup>* disrupts expression of  
152 *si:dkey234h16.7* or neighbouring genes, we performed quantitative analysis of gene transcript  
153 levels in wild type and mutant *dmist* larvae by RT-qPCR. This revealed that the *dmist* viral  
154 insertion caused a more than 70% reduction in the expression of *si:dkey234h16.7* while the  
155 expression of the most proximal 5' or 3' flanking genes, *slc6a4b\_Dr* and *ankrd13a\_Dr*, were  
156 unaffected (Figure 2B and S3A). Since this reduced expression is most consistent with  
157 *si:dkey234h16.7* being the causal lesion of the *dmist* mutant sleep phenotype, we renamed  
158 this gene *dreammist* (*dmist*).

159 Computational predictions indicated that the *dmist* transcripts contain a small open reading  
160 frame (ORF) encoding a protein of 70 amino acids (aa) (Figure 2C). Querying the human and  
161 vertebrate protein databases by BLASTp using the C-terminal protein sequence of Dmist  
162 identified orthologs in most vertebrate clades, including other species of teleost fish, birds,

163 amphibians, and mammals (Figure 2A, C). All identified orthologs encoded predicted proteins  
164 with an N-terminal signal peptide sequence and a C-terminal transmembrane domain (Figure  
165 2C). The peptide sequence identity across orthologs ranged from 38 to 84%, with three peptide  
166 motifs (QNLV, CVYKP, RRR) showing high conservation across all vertebrates, and high  
167 similarity for many additional residues (Figure 2C, Figure S3D). Additional searches by  
168 tBLASTn failed to identify any non-vertebrate *dmist* orthologs. In summary, we found that the  
169 *dreammist* gene, the expression of which is disrupted in *dmist<sup>vir/vir</sup>* fish with sleep phenotypes,  
170 encodes a protein of uncharacterized function that is highly conserved across vertebrates at  
171 both the genomic and molecular levels.

172

### 173 **Genetic molecular analysis of *dmist* expression in zebrafish and mouse**

174 Because the viral insertion disrupts *dmist* throughout the animal's lifetime, we examined  
175 both the developmental and spatial expression of *dmist* to assess when and where its function  
176 may be required for normal sleep. Using the full-length transcript as a probe (Figure S3B), we  
177 performed *in situ* hybridization across embryonic and larval zebrafish development. Maternally  
178 deposited *dmist* was detected in early embryos (2-cell stage) prior to the maternal to zygotic  
179 transition (Giraldez et al., 2006) (Figure 2D). Consistent with maternal deposition of *dmist*  
180 transcripts, inspection of the 3' end of the *dmist* gene revealed a cytoplasmic polyadenylation  
181 element ('TTTTTTAT'; Supplemental Information 2) that is required for zygotic translation of  
182 maternal transcripts (Villalba et al., 2011). At 24 hpf, transcripts were detected in regions that  
183 form the embryonic brain, such as ventral telencephalon, diencephalon and cerebellum, and  
184 in the developing eye (Figure 2D, S3C). By 5 dpf, *dmist* transcripts were detected throughout  
185 the brain (Figure 2D). To test whether *dmist* transcripts are under circadian regulation, we  
186 performed RT-qPCR in fish that were entrained and then shifted to free-running constant dark  
187 conditions. In contrast with the robust 24-hr rhythmic transcription of the circadian clock gene

188 *per1*, we did not detect any changes in *dmist* expression throughout the 24 hour circadian cycle  
189 (Figure S2D).

190 Consistent with brain expression in larval zebrafish, we identified the expression of  
191 *Dmist\_Mm* in a published RNAseq dataset of six isolated cell types from mouse cortex (Zhang  
192 et al., 2014). We confirmed that *Dmist\_Mm* is specifically enriched in neurons by hierarchical  
193 clustering of all 16,991 expressed transcripts across all six cell types, which demonstrated  
194 that *Dmist\_Mm* co-clusters with neuronal genes (Figure S3E). Pearson correlation of  
195 *Dmist\_Mm* with canonical markers for the six cell types showed that *Dmist\_Mm* expression is  
196 highly correlated with other neuronal genes but not genes associated with microglia,  
197 oligodendrocytes, or endothelia. This result indicates that *dmist* is specifically expressed in  
198 neurons in both zebrafish and mouse (Figure S3F).

199

## 200 **Dmist localises to the plasma membrane**

201 Although the *dmist* gene encodes a conserved ORF with a predicted signal peptide  
202 sequence and transmembrane domain (Figure 2C; Figure S3G-I), we wanted to confirm this  
203 small peptide can localise to the membrane and if so, on which cellular compartments. To test  
204 these computational predictions, we transiently co-expressed GFP-tagged Dmist (C-terminal  
205 fusion) with a marker for the plasma membrane (myr-Cherry) in zebrafish embryos. Imaging at  
206 90% epiboly revealed Dmist-GFP localised to the plasma membrane (Figure 2E). Conversely,  
207 introducing a point mutation into Dmist's signal peptide cleavage site (DmistA22W-GFP)  
208 prevented Dmist from trafficking to the plasma membrane, with likely retention in the  
209 endoplasmic reticulum (Figure 2F). Together, these data indicate that Dmist localises to the  
210 plasma membrane despite its small size, as computationally predicted.

211

## 212 **CRISPR/Cas9 generated *dmist*<sup>i8</sup> mutant exhibits decreased night-time sleep**

213 *dmist* expression was reduced by 70% in the viral insertion line, suggesting that *dmist<sup>vir</sup>* is a  
214 hypomorphic allele. To confirm that the sleep phenotypes observed in *dmist<sup>vir/vir</sup>* animals are  
215 due to the loss of Dmist function, we used CRISPR/Cas9 to create an independent *dmist* loss  
216 of function allele. We generated a zebrafish line in which the *dmist* gene contains an 8 bp  
217 insertion that causes a frameshift and early stop codon (*dmist<sup>i8</sup>*, Figure 3A). The *dmist<sup>i8</sup>* allele  
218 is predicted to encode a truncated protein lacking the complete signal peptide sequence and  
219 transmembrane domain (Figure 3B), indicating this is likely a null allele. RT-qPCR showed that  
220 *dmist* transcript levels were 60% lower in *dmist<sup>i8/i8</sup>* fish compared to wild type siblings,  
221 consistent with nonsense-mediated decay (Figure S4A, B) (Wittkopp et al., 2009).

222 We next assessed the sleep and activity patterns of *dmist<sup>i8/i8</sup>* fish. As seen in exemplar  
223 individual tracking experiments, *dmist<sup>i8/i8</sup>* larvae sleep less at night due to fewer sleep bouts  
224 and also show an increase in waking activity relative to wild type and heterozygous mutant  
225 siblings (Figure 3C-H). This significant night-time reduction in sleep and increase in  
226 hyperactivity is also apparent when combining 5 independent experiments with a linear mixed  
227 effects (LME) model to normalize behaviour across datasets (Figure 3I). Although *dmist<sup>vir/vir</sup>*  
228 larvae also sleep less at night (Figure 1G), the large day-time reduction in sleep observed in  
229 *dmist<sup>vir/vir</sup>* larvae is absent in *dmist<sup>i8/i8</sup>* animals, perhaps due to differences in genetic  
230 background that affect behaviour. Because the *dmist<sup>vir</sup>* is likely a hypomorphic allele, we  
231 focused subsequent experiments on the CRISPR-generated *dmist<sup>i8/i8</sup>* larvae.

232 To test whether the increased night-time activity of *dmist<sup>i8/i8</sup>* mutants persists in older  
233 animals, we raised *dmist<sup>i8/i8</sup>* mutants with their heterozygous and wild type siblings to adulthood  
234 in the same tank and tracked individual behaviour for several days on a 14:10 light:dark cycle.  
235 As in larval stages, *dmist<sup>i8/i8</sup>* adults were hyperactive relative to both *dmist<sup>i8/+</sup>* and *dmist<sup>+/+</sup>*  
236 siblings, maintaining a higher mean speed at night (Figure 3J-L). This suggests that either  
237 Dmist affects a sleep/wake regulatory circuit during development that is permanently altered in

238 *dmist* mutants, or that *Dmist* is continuously required to maintain normal levels of night-time  
239 locomotor activity.

240

### 241 ***Dmist* is distantly related to the Na<sup>+</sup>/K<sup>+</sup> pump regulator *Fxyd1* (Phospholemman)**

242 Because *Dmist* is a small, single pass transmembrane domain protein without any clear  
243 functional motifs and has not been functionally characterized in any species, we searched for  
244 similar peptides that might provide clues for how *Dmist* regulates behaviour. Using the multiple  
245 sequence alignment tool MAFFT to align the zebrafish, mouse, and human *Dmist* peptides  
246 (Kato and Toh, 2010) and seeding a hidden Markov model iterative search (JackHMMER) of  
247 the Uniprot database (Johnson et al., 2010), we found distant homology between *Dmist* and  
248 *Fxyd1*/Phospholemman (Figure 4A), a small transmembrane domain peptide that regulates ion  
249 channels and pumps, including the Na<sup>+</sup>,K<sup>+</sup>-ATPase pump (Crambert et al., 2002). *Dmist* and  
250 *Fxyd1* share 27-34% amino acid homology, including an RRR motif at the C-terminal end,  
251 although *Dmist* lacks a canonical FXYD sequence (Figure 4A). In addition, computational  
252 predictions using the AlphaFold protein structure database revealed structural similarities  
253 between *Dmist* and *Fxyd1* (Jumper et al., 2021), suggesting that *Dmist* may belong to a class  
254 of small, single pass transmembrane ion pump regulators.

255 Using *In situ* hybridisation, we found that *fxyd1* is expressed in cells along the brain ventricle  
256 and choroid plexus (Figure 4C) in contrast to the neuronal expression of *dmist* (Figure 2D).  
257 Despite these different expression patterns, based on their sequence similarity we reasoned  
258 that *Fxyd1* and *Dmist* may regulate the same molecular processes that are involved in sleep.  
259 To test this hypothesis, we used CRISPR/Cas9 to generate a 28 bp deletion in the third exon  
260 of the zebrafish *fxyd1* gene, causing a frameshift that is predicted to encode a truncated protein  
261 that lacks the FXYD, transmembrane, and C-terminal domains (Figure 4B). Contrary to a  
262 previous report based on morpholino knockdown (Chang et al., 2012), *fxyd1*<sup>Δ28/Δ28</sup> larvae were



263 viable with no detectable defect in inflation of the brain ventricles. We therefore tested *fxyd1*  
264 mutant larvae for sleep phenotypes. Like *dmist* mutants, *fxyd1*<sup>A28/Δ28</sup> larvae slept less at night  
265 (Figure 4D-F). Interestingly, this sleep loss is mainly due to shorter sleep bouts (Figure 4F),  
266 indicating that *fxyd1* mutants initiate sleep normally but do not properly maintain it, unlike *dmist*  
267 mutants, which initiate fewer night-time sleep bouts, although in both cases there is  
268 consolidation of the wake state at night (Figure 3I, 4F). Thus, despite the non-neuronal  
269 expression of *fxyd1* in the brain, mutation of the gene most closely related to *dmist* results in a  
270 similar sleep phenotype.

271

## 272 **The brain-wide Na<sup>+</sup>/K<sup>+</sup> pump alpha subunit Atp1a3a regulates sleep at night**

273 Given the similarity between Dmist and Fxyd1 and their effects on night-time sleep, we  
274 hypothesized that mutations in Na<sup>+</sup>/K<sup>+</sup> pump subunits known to interact with Fxyd1 might also  
275 affect sleep. Consistent with this hypothesis, a low dose of the Na<sup>+</sup>/K<sup>+</sup> pump inhibitor, ouabain,  
276 reduced night-time sleep in dose-response studies (Figure S5A). When applied in the late  
277 afternoon of 6 dpf, 1 μM ouabain decreased subsequent night-time sleep by 16.5% relative to  
278 controls, an effect size consistent with those observed in *dmist* mutants (Figure 5A, C). Night-  
279 time waking activity was also significantly increased after low-dose ouabain exposure (Figure  
280 5B, D). Ouabain binds to specific sites within the first extracellular domain of Na<sup>+</sup>/K<sup>+</sup> pump  
281 alpha subunits (Price and Lingrel, 1988), and species-specific changes to these sites confers  
282 species-specific ouabain resistance, as in the case of two naturally occurring amino acid  
283 substitutions present in the Atp1a1 subunit of mice (Dostanic et al., 2004). Alignment of the  
284 ouabain sensitive region of zebrafish and mouse Na<sup>+</sup>/K<sup>+</sup> pump alpha subunits revealed that  
285 zebrafish Atp1a1a lacks the conserved Glutamine at position 121 (Figure 5E), suggesting that  
286 one of the other subunits with conserved ouabain-binding sites is responsible for the low dose  
287 ouabain sleep effects. We focused on the Na<sup>+</sup>/K<sup>+</sup> pump alpha-3 subunit (Atp1a3), as this has



288 been shown to directly interact with Fxyd1 in mammalian brain tissue (Feschenko et al., 2003).  
289 Murine *Dmist* expression also correlates well with the *Atp1a3* distribution across 5 brain cell  
290 types in mouse (Pearson correlation coefficient = 0.63), which has the strongest correlation  
291 score with neuronal markers (Figure S5B compared to Figure S3F). In contrast, zebrafish  
292 *atp1a2a* is reportedly expressed in muscle at larval stages, while *atp1a1b* is confined to cells  
293 along the ventricle (Thisse et al., 2001).

294 Zebrafish have two *Atp1a3* paralogs, *atp1a3a* and *atp1a3b*. Similar to *dmist*, *atp1a3a* is  
295 widely expressed in the larval zebrafish brain (Figure 5F, compare to Figure 2D). While *atp1a3b*  
296 is also expressed in the zebrafish brain, its expression is more limited to regions of the midbrain  
297 and hindbrain (Figure S5C). To test whether these genes are involved in regulating zebrafish  
298 sleep, we used CRISPR/Cas9 to isolate an allele of *atp1a3a* containing a 19 bp deletion and  
299 an allele of *atp1a3b* containing a 14 bp deletion. Both mutations are predicted to generate null  
300 alleles due to deletion of the start codon (Figure 5G, S5D). Both *atp1a3a*<sup>Δ19/Δ19</sup> and  
301 *atp1a3b*<sup>Δ14/Δ14</sup> mutant larvae were healthy and viable through early development, although  
302 *atp1a3b* mutant larvae were not obtained at Mendelian ratios (55 wild type [52.5 expected],  
303 142 [105] *atp1a3b*<sup>+/-</sup>, 13 [52.5] *atp1a3b*<sup>-/-</sup>; p<0.0001, Chi-squared), suggesting some impact on  
304 early stages of development leading to lethality. Contrary to a previous report based on  
305 morpholino injections (Doğanli et al., 2013), neither mutant had defects in the inflation of their  
306 brain ventricles. Sleep-wake tracking experiments found that *atp1a3b*<sup>Δ14/Δ14</sup> mutants were more  
307 active during the day with minimal sleep phenotypes (Figure S5E-G). In contrast, mutation of  
308 *atp1a3a* resulted in large effects on sleep-wake behaviour. Compared to wild type and  
309 heterozygous mutant siblings, *atp1a3a*<sup>Δ19/Δ19</sup> animals were hyperactive throughout the day and  
310 night and had a large reduction in sleep at night (Figure 5H, I). The night-time sleep reduction  
311 was due to a reduction in the length of sleep bouts, as *atp1a3a* mutants even had a small  
312 increase in the number of sleep bouts at night (Figure 5J). In conclusion, loss of *atp1a3a* results

313 in sleep loss at night, similar to treatment with the small molecule *ouabain*, and to *dmist* and  
314 *fxyd1* mutants. Notably, the *atp1a3a* mutant phenotype is much stronger, as might be expected  
315 if Dmist plays a modulatory, and Atp1a3a a more central, role in Na<sup>+</sup>/K<sup>+</sup> pump activity.

316

### 317 **Dmist modulates Na<sup>+</sup>/K<sup>+</sup> pump function and neuronal activity-induced sleep** 318 **homeostasis**

319 The similar night-time reduction in sleep in *dmist* and *atp1a3a* mutants, combined with the  
320 similarities between Dmist and Fxyd1, suggested that Dmist may regulate the Na<sup>+</sup>/K<sup>+</sup> pump.  
321 We therefore exposed wild type and mutant larvae to pentylentetrazol (PTZ), a GABA-  
322 receptor antagonist that leads to globally heightened neuronal activity and elevated intracellular  
323 sodium levels that must be renormalized by Na<sup>+</sup>/K<sup>+</sup> pump activity. Consistent with the  
324 hypothesis that Dmist and Atp1a3a subunits are important for a fully functional Na<sup>+</sup>/K<sup>+</sup> pump,  
325 brains from both *dmist*<sup>i8/i8</sup> and *atp1a3a*<sup>A19/A19</sup> larvae had elevated intracellular sodium levels  
326 after exposure to PTZ (Figure 6A). Thus, neither *dmist* nor *atp1a3a* mutants were able to  
327 restore intracellular sodium balance after sustained neuronal activity as quickly as wild type  
328 siblings. Consistent with the night-specific alterations in sleep behaviour, we also found that  
329 baseline brain Na<sup>+</sup> levels in *dmist* mutants were significantly elevated at night but not during  
330 the day (Figure 6B). Collectively, these data are consistent with the hypothesis that night-time  
331 sleep duration is affected by changes in Na<sup>+</sup>/K<sup>+</sup> pump function and that Dmist is required to  
332 maintain this function both at night and after sustained high levels of neuronal activity.

333 We have previously shown in zebrafish that a brief exposure to hyperactivity-inducing drugs  
334 such as the epileptogenic PTZ or wake-promoting caffeine induces a dose-dependent increase  
335 in homeostatic rebound sleep following drug washout that is phenotypically and mechanistically  
336 similar to rebound sleep following physical sleep deprivation (Reichert et al., 2019). Based on

337 their exaggerated intracellular Na<sup>+</sup> levels following exposure to PTZ, we predicted that *dmist*  
338 mutants would also have increased rebound sleep in response to heightened neuronal activity.  
339 Upon wash-on/wash-off of lower dose (5 mM) PTZ, sleep rebound occurs in approximately  
340 50% of wild type larvae (Reichert et al., 2019; Figure 6C, D). In contrast, all *dmist*<sup>#8/i8</sup> larvae  
341 showed increased rebound sleep compared to *dmist*<sup>+/+</sup> sibling controls (Figure 6C-E). Taken  
342 together with the elevated sodium retention experiments, such increases in rebound sleep  
343 induced by neuronal activity suggests that *dmist*<sup>#8/i8</sup> fish more rapidly accumulate sleep  
344 pressure in response to heightened neuronal activity.

345 Finally, we predicted that if Dmist is affecting baseline sleep via modulation of Atp1a3a-  
346 containing Na<sup>+</sup>/K<sup>+</sup> pumps, *dmist*<sup>-/-</sup>; *atp1a3a*<sup>-/-</sup> double mutants should have a reduction in night-  
347 time sleep that is not the sum of effects from either mutant alone. In other words, if Dmist and  
348 Atp1a3a are acting in separate pathways, the double mutant would have an additive  
349 phenotype, but if Dmist and Atp1a3a act together in the same complex/pathway, the mutant  
350 phenotypes should be non-additive. Indeed, *dmist*<sup>-/-</sup>; *atp1a3a*<sup>-/-</sup> mutants have a sleep reduction  
351 similar to that of *atp1a3a*<sup>-/-</sup> mutants alone, consistent with a non-additive effect (Figure 6F and  
352 S6). Similar non-additivity can be also observed in the *dmist*<sup>-/-</sup>; *atp1a3a*<sup>+/-</sup> animals, which, like  
353 *atp1a3a*<sup>+/-</sup> animals alone, have a milder sleep reduction, indicating that the lack of additivity  
354 between *dmist* and *atp1a3a* phenotypes is unlikely due to a floor effect, since double  
355 homozygous mutants can sleep even less (Figure 6F). This genetic interaction data is  
356 consistent with our hypothesis that Atp1a3a and Dmist act in the same pathway—the Na<sup>+</sup>/K<sup>+</sup>  
357 pump-- to influence sleep.

358

## 359 **DISCUSSION**

### 360 **Genetic screening discovers *dmist*, a novel sleep-regulatory gene**

361 Using a reverse genetic viral screening strategy, we discovered a short-sleeping mutant,  
362 *dmist*, which has a disruption in a previously uncharacterized gene encoding a small  
363 transmembrane peptide. Given that the *dmist* mutant appeared within the limited number of 26  
364 lines that we screened, it is likely that many other sleep genes are still waiting to be discovered  
365 in future screens. In zebrafish, one promising screening strategy will be to employ  
366 CRISPR/Cas9 genome editing to systematically target candidate genes. Advances in the  
367 efficiency of this technology now makes it feasible to perform a CRISPR “F0 screen” in which  
368 the consequences of bi-allelic, gene-specific mutations are rapidly tested in the first generation,  
369 with only the most promising lines pursued in germline-transmitted mutant lines (Grunwald et  
370 al., 2019; Jao et al., 2013; Kroll et al., 2021; Shah et al., 2015; Shankaran et al., 2017; Wu et  
371 al., 2018). CRISPR F0 screens could be scaled to systematically target the large number of  
372 candidate sleep-regulatory genes identified through human GWAS studies and sequencing of  
373 human patients suffering from insomnia and neuropsychiatric disorders (Allebrandt et al., 2013;  
374 Dashti et al., 2019; Jansen et al., 2019; Jones et al., 2019; Lane et al., 2019; Lek et al., 2016;  
375 Palagini et al., 2019).

### 376 377 **Dmist is related to the Na<sup>+</sup>/K<sup>+</sup> pump regulator Fxyd1**

378 The small Dmist transmembrane protein is highly conserved across vertebrates, expressed  
379 in neurons, and important for maintaining normal sleep levels. How can such a small, single  
380 pass transmembrane protein lacking any clear functional domains modulate the function of  
381 neurons and ultimately animal behaviour? The recognition that Dmist has sequence homology  
382 (~35% amino acid similarity; a conserved ‘RRR’ motif in the C-terminus) and structural  
383 homology (e.g. signal peptide and single pass transmembrane domains) to the Na<sup>+</sup>,K<sup>+</sup>-ATPase  
384 pump regulator Fxyd1 (Phospholemman) offers some important clues.

385 Fxyd1/Phospholemman is a member of the FXYD protein family, of which there are seven  
386 mammalian members (Sweadner and Rael, 2000). Each of the FXYD proteins is small,  
387 contains a characteristic FXYD domain, and has a single transmembrane domain. FXYD family  
388 members interact with alpha subunits of the Na<sup>+</sup>,K<sup>+</sup> ATPase to regulate the function of this  
389 pump, with individual family members expressed in different tissues to modulate Na<sup>+</sup>,K<sup>+</sup>-  
390 ATPase activity depending on the physiological needs of the tissue (Geering et al., 2003). In  
391 cardiac muscle, FXYD1 is thought to act as a hub through which various signalling cascades,  
392 such as PKA, PKC, or nitric oxide, can activate or inhibit Na<sup>+</sup> pump activity (Pavlovic et al.,  
393 2013). For example, FXYD1 is critical for mediating the increased Na<sup>+</sup> pump activity observed  
394 after β-receptor stimulation via cAMP-PKA signalling (Despa et al., 2008). Much less is known  
395 about the role of FXYD1 in non-cardiac tissue, although it is expressed in neurons in the  
396 mammalian cerebellum, the choroid plexus, and ependymal cells, where it interacts with all  
397 three alpha subunits of the Na<sup>+</sup>,K<sup>+</sup> ATPase (Feschenko et al., 2003).

398 In zebrafish, we also found that *fxyd1* is expressed in cells around the ventricles and in the  
399 choroid plexus (Figure 4C), in contrast to *dmist* which is expressed in neurons throughout the  
400 brain. Despite the different expression patterns, mutation of each gene resulted in a similar  
401 reduction of sleep at night. However, unlike *dmist* mutants, which have fewer sleep bouts (i.e.  
402 initiate sleep less) and an increase in waking locomotor activity, *fxyd1* mutants have shorter  
403 sleep bouts (i.e. cannot maintain sleep) on average and do not have a locomotor activity  
404 phenotype. Just as the various FXYD family members modulate the Na<sup>+</sup>/K<sup>+</sup> pump in different  
405 tissue- and context-specific ways, this phenotypic variation between *fxyd1* and *dmist* mutants  
406 could be due to the different *fxyd1* and *dmist* expression patterns, modulation kinetics of  
407 pump/channel dynamics, or interaction with different accessory proteins or signal transduction  
408 cascades. Nevertheless, the similar timing and magnitude of sleep reduction, combined with

409 the structural similarity of Fxyd1 and Dmist, suggest that they may regulate similar sleep-  
410 related processes.

411

## 412 **Dmist, the sodium pump, and sleep**

413 The similarity between Dmist and FXYD1 led us to directly manipulate the Na<sup>+</sup>,K<sup>+</sup> ATPase  
414 to test its importance in sleep. The Na<sup>+</sup>,K<sup>+</sup>-ATPase is the major regulator of intracellular Na<sup>+</sup> in  
415 all cells and, by actively exchanging two imported K<sup>+</sup> ions for three exported Na<sup>+</sup> ions, is  
416 essential for determining cellular resting membrane potential (reviewed in Clausen et al.,  
417 2017). The Na<sup>+</sup>,K<sup>+</sup>-ATPase consists of a catalytic alpha subunit (4 known isoforms, ATP1A1-  
418 4), a supporting beta subunit (3 isoforms, ATP1B1-3), and a regulatory gamma subunit (the  
419 FXYD proteins). The alpha1 and alpha3 subunits are the predominant catalytic subunits in  
420 neurons (alpha2 is mostly restricted to glia), although the alpha1 subunit is also used  
421 ubiquitously in all tissues (McGrail et al., 1991). By mutating zebrafish orthologs of *Atp1a3*, we  
422 therefore could test the neuronal-specific role of the Na<sup>+</sup>,K<sup>+</sup>-ATPase in sleep.

423 Mutations in both zebrafish *Atp1a3* orthologs increased waking locomotor behaviour during  
424 the day. However, only mutations in *atp1a3a*, which is expressed brain-wide, but not in  
425 *atp1a3b*, which is expressed in more restricted brain regions, led to changes in night-time  
426 sleep. The *atp1a3a* mutants have a larger sleep reduction than *dmist<sup>vir</sup>*, *dmist<sup>i8</sup>*, or *fxyd1<sup>A28</sup>*  
427 mutants, which is expected since loss of a pump subunit should have a larger effect than the  
428 loss of a modulatory subunit, as has been shown for other ion channels (Cirelli et al., 2005;  
429 Wu et al., 2014). Autosomal dominant missense mutations leading to loss of function in  
430 *ATP1A3* cause movement disorders such as rapid-onset dystonia parkinsonism and childhood  
431 alternating hemiplegia (recurrent paralysis on one side) in humans (Canfield et al., 2002;  
432 Heinzen et al., 2014), while loss of function mutations in *Atp1a3* result in generalised seizures

433 and locomotor abnormalities, including hyperactivity, in mice, which was not observed in  
434 zebrafish (Clapcote et al., 2009; Hunanyan et al., 2015; Ikeda et al., 2013; Kirshenbaum et al.,  
435 2011; Sugimoto et al., 2014). A very high prevalence of insomnia was recently reported in  
436 patients with childhood alternating hemiplegia, some of which harboured mutations in *Atp1a3*  
437 (Kansagra et al., 2019), consistent with our observations that insomnia at night is a direct  
438 behavioural consequence of *atp1a3a* mutation in zebrafish. Since zebrafish *atp1a3a* mutants  
439 phenocopy the insomnia and hyperactivity phenotypes observed in patients, small molecule  
440 screens aimed at ameliorating zebrafish *atp1a3a* mutant phenotypes may be a promising  
441 approach for the rapid identification of new therapies for the management of this disease  
442 (Hoffman et al., 2016; Rihel et al., 2010).

443 Together, the night-specific sleep phenotypes of *dmist*, *fyxd1*, and *atp1a3a* mutants point to  
444 a role for the Na<sup>+</sup>,K<sup>+</sup>-ATPase in boosting sleep at night. How might the alpha3 catalytic subunit  
445 of the Na<sup>+</sup>/K<sup>+</sup> pump regulate sleep, and how could Dmist be involved? We found that Dmist is  
446 required for proper maintenance of brain intracellular Na<sup>+</sup> levels at night but not during the day,  
447 mirroring the timing of sleep disruption in *dmist<sup>i8/i8</sup>* animals. This suggests that the decreased  
448 night-time sleep of *dmist* mutants is due to a specific requirement for Dmist modulation of the  
449 Na<sup>+</sup>/K<sup>+</sup> pump at night. However, we cannot exclude the possibility that Dmist's function is  
450 required in only a subset of critical sleep/wake regulatory neurons during the day that then  
451 influence behaviour at night, such as the wake-active, sleep-homeostatic regulating  
452 serotonergic neurons of the raphe (Oikonomou et al., 2019) or wake-promoting Hcrt/orexin  
453 neurons (Li et al., 2022). We also cannot exclude a role for Dmist and the Na<sup>+</sup>/K<sup>+</sup> pump in  
454 developmental events that impact sleep, although our observation that ouabain treatment,  
455 which inhibits the pump acutely after early development is complete, also impacts sleep,  
456 argues against a developmental role. Another possibility is that disruption of proper  
457 establishment of the Na<sup>+</sup> electrochemical gradient in *dmist* mutant neurons leads to dysfunction



458 of various neurotransmitter reuptake transporters, including those for glycine, GABA,  
459 glutamate, serotonin, dopamine, and norepinephrine, which rely on energy from the Na<sup>+</sup>  
460 gradient to function (Kristensen et al., 2011).

461 A third possibility is that *Dmist* and the Na<sup>+</sup>,K<sup>+</sup>-ATPase regulate sleep not by modulation of  
462 neuronal activity per se but rather via modulation of extracellular ion concentrations. Recent  
463 work has demonstrated that interstitial ions fluctuate across the sleep/wake cycle in mice. For  
464 example, extracellular K<sup>+</sup> is high during wakefulness, and cerebrospinal fluid containing the ion  
465 concentrations found during wakefulness directly applied to the brain can locally shift neuronal  
466 activity into wake-like states (Ding et al., 2016). Given that the Na<sup>+</sup>,K<sup>+</sup>-ATPase actively  
467 exchanges Na<sup>+</sup> ions for K<sup>+</sup>, the high intracellular Na<sup>+</sup> levels we observe in *atp1a3a* and *dmist*  
468 mutants is likely accompanied by high extracellular K<sup>+</sup>. Although we can only speculate at this  
469 time, a model in which extracellular ions that accumulate during wakefulness and then directly  
470 signal onto sleep-regulatory neurons could provide a direct link between Na<sup>+</sup>,K<sup>+</sup> ATPase  
471 activity, neuronal firing, and sleep homeostasis. Such a model could also explain why  
472 disruption of *fxyd1* in non-neuronal cells also leads to a reduction in night-time sleep.

473 In addition to decreased night-time sleep, we also observed that *dmist* mutants have an  
474 exaggerated sleep rebound response following the high, widespread neuronal activity induced  
475 by the GABA-receptor antagonist, PTZ. Since both *Atp1a3a* and *Dmist* were essential for re-  
476 establishing proper brain intracellular Na<sup>+</sup> levels following PTZ exposure (Figure 6A), we  
477 speculate that the exaggerated sleep rebound is a consequence of increased neuronal  
478 depolarization due to defective Na<sup>+</sup> pump activity. This is consistent with our previous  
479 observations that the intensity of brain-wide neuronal activity impacts the magnitude of  
480 subsequent sleep rebound via engagement of the Galanin sleep-homeostatic output arm  
481 (Reichert et al., 2019). Why does loss of *dmist* lead to both decreased night-time sleep and  
482 increased sleep rebound in response to exaggerated neuronal activity during the day? One



483 possibility is that Na<sup>+</sup>/K<sup>+</sup> pump complexes made up of different alpha and beta subunits may  
484 be differentially required for maintaining Na<sup>+</sup> homeostasis under physiological conditions and  
485 have different affinities for (or regulation by) Dmist. For example, the Atp1a1 subunit is  
486 considered the Na<sup>+</sup>/K<sup>+</sup> pump workhorse in neurons, while Atp1a3, which has a lower affinity  
487 for Na<sup>+</sup> ions, plays an essential role in repolarizing neurons when Na<sup>+</sup> rapidly increases during  
488 high levels of neuronal activity, such as after a seizure (Azarias et al., 2013). If Dmist  
489 preferentially interacts with Atp1a3a subunit, with which the non-additive effect of *dmist* and  
490 *atp1a3a* mutation on sleep is consistent, day-time sleep-related phenotypes in *dmist* mutants  
491 might be uncovered only during physiological challenge. Conversely, neurons may be more  
492 dependent on Atp1a3a and Dmist for sodium homeostasis at night due to changes in Na<sup>+</sup>/K<sup>+</sup>  
493 pump composition, Dmist interactions, or ion binding affinities. For example, activity of the  
494 Na<sup>+</sup>/K<sup>+</sup> pump can be modulated by the circadian clock (Damulewicz et al., 2013; Nakashima  
495 et al., 2018), changes in substrate availability, including ATP (reviewed in Therien and Blostein,  
496 2000), or hormones (Ewart and Klip, 1995). Teasing out how Dmist modulation of the Na<sup>+</sup>/K<sup>+</sup>  
497 pump changes across the day-night cycle, and in which neurons Dmist's function may be  
498 particularly important at night, will require future investigation.

499 In conclusion, through a genetic screening strategy in zebrafish, we have identified a novel  
500 brain expressed gene that encodes a small transmembrane protein regulator of night-time  
501 sleep and wake behaviours. Future work will be required to uncover the precise signalling  
502 dynamics by which Dmist regulates the Na<sup>+</sup>,K<sup>+</sup>-ATPase and sleep.

503

## 504 **Acknowledgements**

505 The initial screen, discovery, and characterization of *dreammist* was conducted in the lab of  
506 Alexander F Schier at Harvard University. We also would like to thank members of the Rihel  
507 lab and other UCL zebrafish groups for helpful comments on experiments and the manuscript.

508 We thank Shannon Shibata-Germanos for *fxyd1* mutant tracking experiments, John  
509 Parnavalas for reagents, Christine Orengo for help with small peptide sequence searches,  
510 Stuart Peirson for early access to mouse transcriptomic data, and Finn Mango Bamber for the  
511 Pokémon-card inspired *dreammist* name. The work was funded by NIH grants awarded to  
512 Alexander Schier (GM085357 and HL10952505); an ERC Starting Grant (#282027) and  
513 Wellcome Trust Investigator Award (#217150/Z/19/Z) to JR; NIH grant R35 NS122172 to DAP;  
514 and a Grand Challenges PhD studentship to ILB.

515

## 516 REFERENCES

- 517 Aday, A.W., Zhu, L.J., Lakshmanan, A., Wang, J., and Lawson, N.D., 2011. Identification of  
518 cis regulatory features in the embryonic zebrafish genome through large-scale profiling  
519 of H3K4me1 and H3K4me3 binding sites. *Dev. Biol.* 357, 450–462.  
520 <https://doi.org/10.1016/j.ydbio.2011.03.007>
- 521 Allebrandt, K. V, Amin, N., Müller-Myhsok, B., Esko, T., Teder-Laving, M., Azevedo,  
522 R.V.D.M., Hayward, C., van Mill, J., Vogelzangs, N., Green, E.W., et al., 2013. A KATP  
523 channel gene effect on sleep duration: from genome-wide association studies to function  
524 in *Drosophila*. *Mol. Psychiatry* 18, 122–132. <https://doi.org/10.1038/mp.2011.142>
- 525 Azarias, G., Kruusmägi, M., Connor, S., Akkuratov, E.E., Liu, X.L., Lyons, D., Brismar, H.,  
526 Broberger, C., and Aperia, A., 2013. A specific and essential role for Na,K-ATPase  $\alpha 3$  in  
527 neurons co-expressing  $\alpha 1$  and  $\alpha 3$ . *J. Biol. Chem.* 288, 2734–2743.  
528 <https://doi.org/10.1074/jbc.M112.425785>
- 529 Barlow, I.L., and Rihel, J., 2017. Zebrafish sleep: from geneZZZ to neuronZZZ. *Curr. Opin.*  
530 *Neurobiol.* 44, 65–71. <https://doi.org/10.1016/j.conb.2017.02.009>
- 531 Bushey, D., Huber, R., Tononi, G., and Cirelli, C., 2007. *Drosophila* Hyperkinetic mutants  
532 have reduced sleep and impaired memory. *J. Neurosci.* 27, 5384–93.  
533 <https://doi.org/10.1523/JNEUROSCI.0108-07.2007>
- 534 Canfield, V.A., Loppin, B., Thisse, B., Thisse, C., Postlethwait, J.H., Mohideen, M.-A.P.,  
535 Rajarao, S.J.R., and Levenson, R., 2002. Na,K-ATPase  $\alpha$  and  $\beta$  subunit genes exhibit  
536 unique expression patterns during zebrafish embryogenesis. *Mech. Dev.* 116, 51–59.

- 537 [https://doi.org/10.1016/S0925-4773\(02\)00135-1](https://doi.org/10.1016/S0925-4773(02)00135-1)
- 538 Chang, J.T., Lowery, L.A., and Sive, H., 2012. Multiple roles for the Na,K-ATPase subunits,  
539 Atp1a1 and Fxyd1, during brain ventricle development. *Dev. Biol.* 368, 312–22.  
540 <https://doi.org/10.1016/j.ydbio.2012.05.034>
- 541 Chemelli, R.M., Willie, J.T., Sinton, C.M., Elmquist, J.K., Scammell, T., Lee, C., Richardson,  
542 J.A., Clay Williams, S., Xiong, Y., Kisanuki, Y., et al., 1999. Narcolepsy in orexin  
543 knockout mice: Molecular genetics of sleep regulation. *Cell* 98, 437–451.  
544 [https://doi.org/10.1016/S0092-8674\(00\)81973-X](https://doi.org/10.1016/S0092-8674(00)81973-X)
- 545 Chew, G.-L., Pauli, A., Rinn, J.L., Regev, A., Schier, A.F., and Valen, E., 2013. Ribosome  
546 profiling reveals resemblance between long non-coding RNAs and 5' leaders of coding  
547 RNAs. *Development* 140, 2828–34. <https://doi.org/10.1242/dev.098343>
- 548 Chiu, C.N., Rihel, J., Lee, D.A., Singh, C., Mosser, E.A., Chen, S., Sapin, V., Pham, U.,  
549 Engle, J., Niles, B.J., et al., 2016. A Zebrafish Genetic Screen Identifies Neuromedin U  
550 as a Regulator of Sleep/Wake States. *Neuron* 89, 842–856.  
551 <https://doi.org/10.1016/j.neuron.2016.01.007>
- 552 Cirelli, C., 2009. The genetic and molecular regulation of sleep: from fruit flies to humans.  
553 *Nat. Rev. Neurosci.* 10, 549–60. <https://doi.org/10.1038/nrn2683>
- 554 Cirelli, C., Bushey, D., Hill, S., Huber, R., Kreber, R., Ganetzky, B., and Tononi, G., 2005.  
555 Reduced sleep in *Drosophila* Shaker mutants. *Nature* 434, 1087–1092.  
556 <https://doi.org/10.1038/nature03486>
- 557 Clapcote, S.J., Duffy, S., Xie, G., Kirshenbaum, G., Bechard, A.R., Schack, V.R., Petersen,  
558 J., Sinai, L., Saab, B.J., Lerch, J.P., et al., 2009. Mutation I810N in the  $\alpha 3$  isoform of  
559 Na<sup>+</sup>,K<sup>+</sup>-ATPase causes impairments in the sodium pump and hyperexcitability in the  
560 CNS. *Proc. Natl. Acad. Sci. U. S. A.* 106, 14085–14090.  
561 <https://doi.org/10.1073/pnas.0904817106>
- 562 Clausen, M. V, Hilbers, F., and Poulsen, H., 2017. The Structure and Function of the Na,K-  
563 ATPase Isoforms in Health and Disease. *Front. Physiol.* 8, 371.  
564 <https://doi.org/10.3389/fphys.2017.00371>
- 565 Crambert, G., Fuzesi, M., Garty, H., Karlsh, S., and Geering, K., 2002. Phospholemman  
566 (FXD1) associates with Na,K-ATPase and regulates its transport properties. *Proc. Natl.*  
567 *Acad. Sci. U. S. A.* 99, 11476–81. <https://doi.org/10.1073/pnas.182267299>

- 568 Damulewicz, M., Rosato, E., and Pyza, E. (2013). Circadian regulation of the Na<sup>+</sup>/K<sup>+</sup>-  
569 ATPase alpha subunit in the visual system is mediated by the pacemaker and by retina  
570 photoreceptors in *Drosophila melanogaster*. *PLoS One* 8, e73690.
- 571 Dashti, H.S., Jones, S.E., Wood, A.R., Lane, J.M., van Hees, V.T., Wang, H., Rhodes, J.A.,  
572 Song, Y., Patel, K., Anderson, S.G., et al. (2019). Genome-wide association study  
573 identifies genetic loci for self-reported habitual sleep duration supported by  
574 accelerometer-derived estimates. *Nat Commun* 10, 1100.
- 575 De Carvalho Aguiar, P., Sweadner, K.J., Penniston, J.T., Zaremba, J., Liu, L., Caton, M.,  
576 Linzasoro, G., Borg, M., Tijssen, M.A.J., Bressman, S.B., et al., 2004. Mutations in the  
577 Na<sup>+</sup>/K<sup>+</sup>-ATPase  $\alpha$ 3 gene ATP1A3 are associated with rapid-onset dystonia  
578 parkinsonism. *Neuron* 43, 169–175. <https://doi.org/10.1016/j.neuron.2004.06.028>
- 579 Despa, S., Tucker, A.L., and Bers, D.M., 2008. Phospholemman-mediated activation of Na/K-  
580 ATPase limits [Na]<sub>i</sub> and inotropic state during  $\beta$ -adrenergic stimulation in mouse  
581 ventricular myocytes. *Circulation* 117, 1849–1855.  
582 <https://doi.org/10.1161/CIRCULATIONAHA.107.754051>
- 583 Ding, F., O'donnell, J., Xu, Q., Kang, N., Goldman, N., and Nedergaard, M., 2016. Changes  
584 in the composition of brain interstitial ions control the sleep-wake cycle. *Science* (80-. ).  
585 352, 550–555. <https://doi.org/10.1126/science.aad4821>
- 586 Doğanli, C., Beck, H.C., Ribera, A.B., Oxvig, C., and Lykke-Hartmann, K., 2013.  $\alpha$ 3Na<sup>+</sup>/K<sup>+</sup>-  
587 ATPase deficiency causes brain ventricle dilation and abrupt embryonic motility in  
588 zebrafish. *J. Biol. Chem.* 288, 8862–8874. <https://doi.org/10.1074/jbc.M112.421529>
- 589 Dostanic, I., J. Schultz Jel, J. N. Lorenz, and J. B. Lingrel. 2004. 'The alpha 1 isoform of  
590 Na,K-ATPase regulates cardiac contractility and functionally interacts and co-localizes  
591 with the Na/Ca exchanger in heart', *J Biol Chem*, 279: 54053-61. Douglas, C.L.,  
592 Vyazovskiy, V., Southard, T., Chiu, S.-Y., Messing, A., Tononi, G., and Cirelli, C., 2007.  
593 Sleep in *Kcna2* knockout mice. *BMC Biol.* 5, 42. <https://doi.org/10.1186/1741-7007-5-42>
- 594 Ewart, H.S., and Klip, A. (1995). Hormonal regulation of the Na<sup>(+)</sup>-K<sup>(+)</sup>-ATPase:  
595 mechanisms underlying rapid and sustained changes in pump activity. *Am J Physiol* 269,  
596 C295-311.
- 597 Feschenko, M.S., Donnet, C., Wetzel, R.K., Asinovski, N.K., Jones, L.R., and Sweadner,  
598 K.J., 2003. Phospholemman, a single-span membrane protein, is an accessory protein

- 599 of Na,K-ATPase in cerebellum and choroid plexus. *J. Neurosci.* 23, 2161–2169.  
600 <https://doi.org/10.1523/jneurosci.23-06-02161.2003>
- 601 Funato, H., Miyoshi, C., Fujiyama, T., Kanda, T., Sato, M., Wang, Z., Ma, J., Nakane, S.,  
602 Tomita, J., Ikkyu, A., et al., 2016. Forward-genetics analysis of sleep in randomly  
603 mutagenized mice. *Nature* 539, 378–383. <https://doi.org/10.1038/nature20142>
- 604 Gagnon, J.A., Valen, E., Thyme, S.B., Huang, P., Ahkmetova, L., Pauli, A., Montague, T.G.,  
605 Zimmerman, S., Richter, C., and Schier, A.F., 2014. Efficient Mutagenesis by Cas9  
606 Protein-Mediated Oligonucleotide Insertion and Large-Scale Assessment of Single-  
607 Guide RNAs. *PLoS One* 9, e98186. <https://doi.org/10.1371/journal.pone.0098186>
- 608 Gandhi, A. V, Mosser, E.A., Oikonomou, G., and Prober, D.A., 2015. Melatonin Is Required  
609 for the Circadian Regulation of Sleep. *Neuron* 85, 1–7.  
610 <https://doi.org/10.1016/j.neuron.2015.02.016>
- 611 Geering, K., Béguin, P., Garty, H., Karlsh, S., Füzesi, M., Horisberger, J.D., and Crambert,  
612 G., 2003. FXYD proteins: New tissue- and isoform-specific regulators of Na,K-ATPase,  
613 in: *Annals of the New York Academy of Sciences*. New York Academy of Sciences, pp.  
614 388–394. <https://doi.org/10.1111/j.1749-6632.2003.tb07219.x>
- 615 Giraldez, A.J., Mishima, Y., Rihel, J., Grocock, R.J., Van Dongen, S., Inoue, K., Enright, A.J.,  
616 and Schier, A.F., 2006. Zebrafish MiR-430 promotes deadenylation and clearance of  
617 maternal mRNAs. *Science* 312, 75–79. <https://doi.org/10.1126/science.1122689>
- 618 Grunwald, H.A., Gantz, V.M., Poplawski, G., Xu, X.R.S., Bier, E., and Cooper, K.L., 2019.  
619 Super-Mendelian inheritance mediated by CRISPR–Cas9 in the female mouse germline.  
620 *Nature*. <https://doi.org/10.1038/s41586-019-0875-2>
- 621 Heinzen, E.L., Arzimanoglou, A., Brashear, A., Clapcote, S.J., Gurrieri, F., Goldstein, D.B.,  
622 Jóhannesson, S.H., Mikati, M.A., Neville, B., Nicole, S., et al., 2014. Distinct neurological  
623 disorders with ATP1A3 mutations. *Lancet. Neurol.* 13, 503–14.  
624 [https://doi.org/10.1016/S1474-4422\(14\)70011-0](https://doi.org/10.1016/S1474-4422(14)70011-0)
- 625 Heinzen, E.L., Swoboda, K.J., Hitomi, Y., Gurrieri, F., De Vries, B., Tiziano, F.D., Fontaine,  
626 B., Walley, N.M., Heavin, S., Panagiotakaki, E., et al., 2012. De novo mutations in  
627 ATP1A3 cause alternating hemiplegia of childhood. *Nat. Genet.* 44, 1030–1034.  
628 <https://doi.org/10.1038/ng.2358>
- 629 Hoffman, E.J., Turner, K.J., Fernandez, J.M., Cifuentes, D., Ghosh, M., Ijaz, S., Jain, R.A.,

- 630 Kubo, F., Bill, B.R., Baier, H., et al., 2016. Estrogens Suppress a Behavioral Phenotype  
631 in Zebrafish Mutants of the Autism Risk Gene, CNTNAP2. *Neuron* 89, 725–733.  
632 <https://doi.org/10.1016/j.neuron.2015.12.039>
- 633 Hunanyan, A.S., Fainberg, N.A., Linabarger, M., Arehart, E., Leonard, A.S., Adil, S.M.,  
634 Helseth, A.R., Swearingen, A.K., Forbes, S.L., Rodriguiz, R.M., et al., 2015. Knock-in  
635 mouse model of alternating hemiplegia of childhood: Behavioral and electrophysiologic  
636 characterization. *Epilepsia* 56, 82–93. <https://doi.org/10.1111/epi.12878>
- 637 Iannacone, M.J., Beets, I., Lopes, L.E., Churgin, M.A., Fang-Yen, C., Nelson, M.D., Schoofs,  
638 L., and Raizen, D.M., 2017. The RFamide receptor DMSR-1 regulates stress-induced  
639 sleep in *C. elegans*. *Elife* 6. <https://doi.org/10.7554/eLife.19837>
- 640 Ikeda, K., Satake, S., Onaka, T., Sugimoto, H., Takeda, N., Imoto, K., and Kawakami, K.,  
641 2013. Enhanced inhibitory neurotransmission in the cerebellar cortex of *Atp1a3*-deficient  
642 heterozygous mice. *J. Physiol.* 591, 3433–3449.  
643 <https://doi.org/10.1113/jphysiol.2012.247817>
- 644 Jansen, P.R., Watanabe, K., Stringer, S., Skene, N., Bryois, J., Hammerschlag, A.R., de  
645 Leeuw, C.A., Benjamins, J.S., Muñoz-Manchado, A.B., Nagel, M., et al., 2019. Genome-  
646 wide analysis of insomnia in 1,331,010 individuals identifies new risk loci and functional  
647 pathways. *Nat. Genet.* 51, 394–403. <https://doi.org/10.1038/s41588-018-0333-3>
- 648 Jao, L.-E., Wenthe, S.R., and Chen, W., 2013. Efficient multiplex biallelic zebrafish genome  
649 editing using a CRISPR nuclease system. *Proc. Natl. Acad. Sci. U. S. A.* 110, 13904–9.  
650 <https://doi.org/10.1073/pnas.1308335110>
- 651 Johnson, L.S., Eddy, S.R., and Portugaly, E., 2010. Hidden Markov model speed heuristic  
652 and iterative HMM search procedure. *BMC Bioinformatics* 11, 431.  
653 <https://doi.org/10.1186/1471-2105-11-431>
- 654 Joiner, W.J., 2016. Unraveling the Evolutionary Determinants of Sleep. *Curr. Biol.* 26,  
655 R1073–R1087. <https://doi.org/10.1016/j.cub.2016.08.068>
- 656 Jones, S.E., van Hees, V.T., Mazzotti, D.R., Marques-Vidal, P., Sabia, S., van der Spek, A.,  
657 Dashti, H.S., Engmann, J., Kocavska, D., Tyrrell, J., et al. (2019). Genetic studies of  
658 accelerometer-based sleep measures yield new insights into human sleep behaviour.  
659 *Nat Commun* 10, 1585.
- 660 Jumper, J., R. Evans, A. Pritzel, T. Green, M. Figurnov, O. Ronneberger, K.



- 661 Tunyasuvunakool, R. Bates, A. Zidek, A. Potapenko, A. Bridgland, C. Meyer, S. A. A.  
662 Kohl, A. J. Ballard, A. Cowie, B. Romera-Paredes, S. Nikolov, R. Jain, J. Adler, T. Back,  
663 S. Petersen, D. Reiman, E. Clancy, M. Zielinski, M. Steinegger, M. Pacholska, T.  
664 Berghammer, S. Bodenstein, D. Silver, O. Vinyals, A. W. Senior, K. Kavukcuoglu, P.  
665 Kohli, and D. Hassabis. 2021. 'Highly accurate protein structure prediction with  
666 AlphaFold', *Nature*, 596: 583-89.
- 667 Kansagra, S., Ghusayni, R., Kherallah, B., Gunduz, T., McLean, M., Prange, L., Kravitz,  
668 R.M., and Mikati, M.A., 2019. Polysomnography findings and sleep disorders in children  
669 with alternating hemiplegia of childhood. *J. Clin. Sleep Med.* 15, 65–70.  
670 <https://doi.org/10.5664/jcsm.7572>
- 671 Katoh, K., and Toh, H., 2010. Parallelization of the MAFFT multiple sequence alignment  
672 program. *Bioinformatics.* <https://doi.org/10.1093/bioinformatics/btq224>
- 673 Kempf, A., Song, S.M., Talbot, C.B., and Miesenböck, G., 2019. A potassium channel  $\beta$ -  
674 subunit couples mitochondrial electron transport to sleep. *Nature* 568, 230–234.  
675 <https://doi.org/10.1038/s41586-019-1034-5>
- 676 Kimmel, C.B., Ballard, W.W., Kimmel, S.R., Ullmann, B., and Schilling, T.F., 1995. Stages of  
677 embryonic development of the zebrafish. *Dev. Dyn.* 203, 253–310.  
678 <https://doi.org/10.1002/aja.1002030302>
- 679 Kirshenbaum, G.S., Clapcote, S.J., Duffy, S., Burgess, C.R., Petersen, J., Jarowek, K.J.,  
680 Yücel, Y.H., Cortez, M.A., Snead, O.C., Vilsen, B., et al., 2011. Mania-like behavior  
681 induced by genetic dysfunction of the neuron-specific Na<sup>+</sup>,K<sup>+</sup>-ATPase  $\alpha$ 3 sodium pump.  
682 *Proc. Natl. Acad. Sci. U. S. A.* 108, 18144–18149.  
683 <https://doi.org/10.1073/pnas.1108416108>
- 684 Koh, K., Joiner, W.J., Wu, M.N., Yue, Z., Smith, C.J., and Sehgal, A., 2009. Identification of  
685 SLEEPLESS, a novel sleep promoting factor. *Science* (80-. ). 321, 372–376.  
686 <https://doi.org/10.1126/science.1155942.Identification>
- 687 Kristensen, A.S., Andersen, J., Jorgensen, T.N., Sorensen, L., Eriksen, J., Loland, C.J.,  
688 Stromgaard, K., and Gether, U., 2011. SLC6 neurotransmitter transporters: Structure,  
689 function, and regulation. *Pharmacol. Rev.* 63, 585–640.  
690 <https://doi.org/10.1124/pr.108.000869>
- 691 Kwan, K.M., Fujimoto, E., Grabher, C., Mangum, B.D., Hardy, M.E., Campbell, D.S., Parant,

- 692 J.M., Yost, H.J., Kanki, J.P., and Chien, C.-B., 2007. The Tol2kit: a multisite gateway-  
693 based construction kit for Tol2 transposon transgenesis constructs. *Dev. Dyn.* 236,  
694 3088–99. <https://doi.org/10.1002/dvdy.21343>
- 695 Lane, J.M., Jones, S.E., Dashti, H.S., Wood, A.R., Aragam, K.G., van Hees, V.T., Strand,  
696 L.B., Winsvold, B.S., Wang, H., Bowden, J., et al. (2019). Biological and clinical insights  
697 from genetics of insomnia symptoms. *Nat Genet* 51, 387-393.
- 698 Lee, D.A., Andreev, A., Truong, T. V., Chen, A., Hill, A.J., Oikonomou, G., Pham, U., Hong,  
699 Y.K., Tran, S., Glass, L., et al., 2017. Genetic and neuronal regulation of sleep by  
700 neuropeptide VF. *Elife* 6. <https://doi.org/10.7554/eLife.25727>
- 701 Lek, M., Karczewski, K.J., Minikel, E. V., Samocha, K.E., Banks, E., Fennell, T., O'Donnell-  
702 Luria, A.H., Ware, J.S., Hill, A.J., Cummings, B.B., et al., 2016. Analysis of protein-  
703 coding genetic variation in 60,706 humans. *Nature* 536, 285–291.  
704 <https://doi.org/10.1038/nature19057>
- 705 Lenz, O., Xiong, J., Nelson, M.D., Raizen, D.M., and Williams, J.A., 2015. FMRFamide  
706 signaling promotes stress-induced sleep in *Drosophila*. *Brain. Behav. Immun.* 47, 141–  
707 148. <https://doi.org/10.1016/j.bbi.2014.12.028>
- 708 Li SB, Damonte VM, Chen C, Wang GX, Kebschull JM, Yamaguchi H, Bian WJ, Purmann C,  
709 Pattni R, Urban AE, Mourrain P, Kauer JA, Scherrer G, de Lecea L. Hyperexcitable arousal  
710 circuits drive sleep instability during aging. *Science*. 2022 Feb 25;375(6583):eabh3021.
- 711 Lin, L., Faraco, J., Li, R., Kadotani, H., Rogers, W., Lin, X., Qiu, X., de Jong, P.J., Nishino, S.,  
712 Mignot, E., et al., 1999. The sleep disorder canine narcolepsy is caused by a mutation in  
713 the hypocretin (orexin) receptor 2 gene. *Cell* 98, 365–76. [https://doi.org/10.1016/S0092-8674\(00\)81965-0](https://doi.org/10.1016/S0092-8674(00)81965-0)
- 715 Love, M.I., Huber, W., and Anders, S., 2014. Moderated estimation of fold change and  
716 dispersion for RNA-seq data with DESeq2. *Genome Biol.* 15, 550.  
717 <https://doi.org/10.1186/s13059-014-0550-8>
- 718 McGrail, K.M., Phillips, J.M., and Sweadner, K.J., 1991. Immunofluorescent localization of  
719 three Na,K-ATPase isozymes in the rat central nervous system: Both neurons and glia  
720 can express more than one Na,K-ATPase. *J. Neurosci.* 11, 381–391.  
721 <https://doi.org/10.1523/jneurosci.11-02-00381.1991>



- 722 Montague, T.G., Cruz, J.M., Gagnon, J.A., Church, G.M., and Valen, E., 2014. CHOPCHOP:  
723 a CRISPR/Cas9 and TALEN web tool for genome editing. *Nucleic Acids Res.* gku410-  
724 <https://doi.org/10.1093/nar/gku410>
- 725 Nakashima, A., Kawamoto, T., Noshiro, M., Ueno, T., Doi, S., Honda, K., Maruhashi, T.,  
726 Noma, K., Honma, S., Masaki, T., et al. (2018). Dec1 and CLOCK Regulate Na(+)/K(+)-  
727 ATPase beta1 Subunit Expression and Blood Pressure. *Hypertension* 72, 746-754.
- 728 Oikonomou, G., Altermatt, M., Zhang, R. wei, Coughlin, G.M., Montz, C., Gradinaru, V., and  
729 Prober, D.A., 2019. The Serotonergic Raphe Promote Sleep in Zebrafish and Mice.  
730 *Neuron* 103, 686-701.e8. <https://doi.org/10.1016/j.neuron.2019.05.038>
- 731 Palagini, L., Domschke, K., Benedetti, F., Foster, R.G., Wulff, K., and Riemann, D., 2019.  
732 Developmental pathways towards mood disorders in adult life: Is there a role for sleep  
733 disturbances? *J. Affect. Disord.* 243, 121–132.  
734 <https://doi.org/10.1016/J.JAD.2018.09.011>
- 735 Pauli, A., Valen, E., Lin, M.F., Garber, M., Vastenhout, N.L., Levin, J.Z., Fan, L., Sandelin,  
736 A., Rinn, J.L., Regev, A., et al., 2012. Systematic identification of long noncoding RNAs  
737 expressed during zebrafish embryogenesis Systematic identification of long noncoding  
738 RNAs expressed during zebrafish embryogenesis 577–591.  
739 <https://doi.org/10.1101/gr.133009.111>
- 740 Pauli, A., Valen, E., and Schier, A.F., 2015. Identifying (non-)coding RNAs and small  
741 peptides: Challenges and opportunities. *BioEssays* 37, 103–112.  
742 <https://doi.org/10.1002/bies.201400103>
- 743 Pavlovic, D., Fuller, W., and Shattock, M.J., 2013. Novel regulation of cardiac Na pump via  
744 phospholemman. *J. Mol. Cell. Cardiol.* 61, 83–93.  
745 <https://doi.org/10.1016/j.yjmcc.2013.05.002>
- 746 Peyron, C., Faraco, J., Rogers, W., Ripley, B., Overeem, S., Charnay, Y., Nevsimalova, S.,  
747 Aldrich, M., Reynolds, D., Albin, R., et al. (2000). A mutation in a case of early onset  
748 narcolepsy and a generalized absence of hypocretin peptides in human narcoleptic  
749 brains. *Nat Med* 6, 991-997.
- 750 Price, E. M., and J. B. Lingrel. 1988. 'Structure-function relationships in the Na,K-ATPase  
751 alpha subunit: site-directed mutagenesis of glutamine-111 to arginine and asparagine-  
752 122 to aspartic acid generates a ouabain-resistant enzyme', *Biochemistry*, 27: 8400-8.

- 753 Prober, D. a, Rihel, J., Onah, A. a, Sung, R.-J., and Schier, A.F., 2006. Hypocretin/orexin  
754 overexpression induces an insomnia-like phenotype in zebrafish. *J. Neurosci.* 26,  
755 13400–10. <https://doi.org/10.1523/JNEUROSCI.4332-06.2006>
- 756 Reichert, S., Pavón Arocas, O., and Rihel, J., 2019. The Neuropeptide Galanin Is Required  
757 for Homeostatic Rebound Sleep following Increased Neuronal Activity. *Neuron* 104, 370-  
758 384.e5. <https://doi.org/10.1016/j.neuron.2019.08.010>
- 759 Rihel, J., Prober, D. a, Arvanites, A., Lam, K., Zimmerman, S., Jang, S., Haggarty, S.J.,  
760 Kokel, D., Rubin, L.L., Peterson, R.T., et al., 2010. Zebrafish behavioral profiling links  
761 drugs to biological targets and rest/wake regulation. *Science* 327, 348–51.  
762 <https://doi.org/10.1126/science.1183090>
- 763 Rihel, J., and Schier, A.F., 2013. Sites of action of sleep and wake drugs: insights from model  
764 organisms. *Curr. Opin. Neurobiol.* 23, 831–40.  
765 <https://doi.org/10.1016/j.conb.2013.04.010>
- 766 Salles, P.A., Mata, I.F., Brunger, T., Lal, D., and Fernandez, H.H. (2021). ATP1A3-Related  
767 Disorders: An Ever-Expanding Clinical Spectrum. *Front Neurol* 12, 637890.
- 768 Sakurai, T., 2013. Orexin deficiency and narcolepsy. *Curr. Opin. Neurobiol.* 23, 760–766.  
769 <https://doi.org/10.1016/j.conb.2013.04.007>
- 770 Sehgal, A., and Mignot, E., 2011. Genetics of sleep and sleep disorders. *Cell* 146, 194–207.  
771 <https://doi.org/10.1016/j.cell.2011.07.004>
- 772 Shah, A.N., Davey, C.F., Whitebirch, A.C., Miller, A.C., and Moens, C.B., 2015. Rapid  
773 reverse genetic screening using CRISPR in zebrafish. *Nat. Methods* 12, 535–540.  
774 <https://doi.org/10.1038/nmeth.3360>
- 775 Shankaran, S.S., Dahlem, T.J., Bisgrove, B.W., Yost, H.J., and Tristani-Firouzi, M., 2017.  
776 CRISPR/Cas9-Directed Gene Editing for the Generation of Loss-of-Function Mutants in  
777 High-Throughput Zebrafish F<sub>0</sub> Screens, in: *Current Protocols in Molecular Biology*. John  
778 Wiley & Sons, Inc., Hoboken, NJ, USA, pp. 31.9.1-31.9.22.  
779 <https://doi.org/10.1002/cpmb.42>
- 780 Singh, C., Oikonomou, G., and Prober, D.A. (2015). Norepinephrine is required to promote  
781 wakefulness and for hypocretin-induced arousal in zebrafish. *Elife* 4, e07000.
- 782 Singh, C., Rihel, J., and Prober, D.A., 2017. Neuropeptide Y Regulates Sleep by Modulating  
783 Noradrenergic Signaling. *Curr. Biol.* 27, 3796-3811.e5.

- 784 <https://doi.org/10.1016/J.CUB.2017.11.018>
- 785 Sivasubbu, S., Balciunas, D., Amsterdam, A., and Ekker, S.C., 2007. Insertional mutagenesis  
786 strategies in zebrafish. *Genome Biol.* <https://doi.org/10.1186/gb-2007-8-s1-s9>
- 787 Sugimoto, H., Ikeda, K., and Kawakami, K., 2014. Heterozygous mice deficient in *Atp1a3*  
788 exhibit motor deficits by chronic restraint stress. *Behav. Brain Res.* 272, 100–110.  
789 <https://doi.org/10.1016/j.bbr.2014.06.048>
- 790 Sweadner, K.J., and Rael, E., 2000. The FXYD gene family of small ion transport regulators  
791 or channels: cDNA sequence, protein signature sequence, and expression. *Genomics*  
792 68, 41–56. <https://doi.org/10.1006/geno.2000.6274>Therien, A.G., and Blostein, R.  
793 (2000). Mechanisms of sodium pump regulation. *Am J Physiol Cell Physiol* 279, C541-  
794 566.
- 795 Thisse, B., Pflumio, S., Fürthauer, M., Loppin, B., Heyer, V., Degrave, A., Woehl, R., Lux, A.,  
796 Steffan, T., Charbonnier, X.Q. and Thisse, C. (2001) Expression of the zebrafish  
797 genome during embryogenesis (NIH R01 RR15402). ZFIN Direct Data Submission. .  
798 (<http://zfin.org>).
- 799 Thisse, C., and Thisse, B., 2008. High-resolution in situ hybridization to whole-mount  
800 zebrafish embryos. *Nat. Protoc.* 3, 59–69. <https://doi.org/10.1038/nprot.2007.514>
- 801 Toda, H., Williams, J.A., Gullede, M., and Sehgal, A., 2019. A sleep-inducing gene, *nemuri*,  
802 links sleep and immune function in *Drosophila*. *Science* 363, 509–515.  
803 <https://doi.org/10.1126/science.aat1650>
- 804 Ulitsky, I., Shkumatava, A., Jan, C.H., Sive, H., and Bartel, D.P., 2011. Conserved function of  
805 lincRNAs in vertebrate embryonic development despite rapid sequence evolution. *Cell*  
806 147, 1537–1550. <https://doi.org/10.1016/j.cell.2011.11.055>
- 807 Varshney, G.K., Lu, J., Gildea, D.E., Huang, H., Pei, W., Yang, Z., Huang, S.C., Schoenfeld,  
808 D., Pho, N.H., Casero, D., et al., 2013. A large-scale zebrafish gene knockout resource  
809 for the genome-wide study of gene function. *Genome Res.* 23, 727–35.  
810 <https://doi.org/10.1101/gr.151464.112>
- 811 Villalba, A., Coll, O., and Gebauer, F., 2011. Cytoplasmic polyadenylation and translational  
812 control. *Curr. Opin. Genet. Dev.* 21, 452–457. <https://doi.org/10.1016/j.gde.2011.04.006>
- 813 Wilkinson, R.N., Elworthy, S., Ingham, P.W., and van Eeden, F.J.M., 2013. A method for  
814 high-throughput PCR-based genotyping of larval zebrafish tail biopsies. *Biotechniques*

815 55, 314–316. <https://doi.org/10.2144/000114116>

816 Wittkopp N, Huntzinger E, Weiler C, Saulière J, Schmidt S, Sonawane M, Izaurralde E.  
817 Nonsense-mediated mRNA decay effectors are essential for zebrafish embryonic  
818 development and survival. *Mol Cell Biol.* 2009 Jul;29(13):3517-28.

819 Wu, M., Robinson, J.E., and Joiner, W.J., 2014. SLEEPLESS Is a Bifunctional Regulator of  
820 Excitability and Cholinergic Synaptic Transmission. *Curr. Biol.* 24, 621–629.  
821 <https://doi.org/10.1016/j.cub.2014.02.026>

822 Wu, R.S., Lam, I.I., Clay, H., Duong, D.N., Deo, R.C., and Coughlin, S.R., 2018. A Rapid  
823 Method for Directed Gene Knockout for Screening in G0 Zebrafish. *Dev. Cell* 46, 112-  
824 125.e4. <https://doi.org/10.1016/j.devcel.2018.06.003>

825 Zhang, Y., Chen, K., Sloan, S.A., Bennett, M.L., Scholze, A.R., O’Keeffe, S., Phatnani, H.P.,  
826 Guarnieri, P., Caneda, C., Ruderisch, N., et al., 2014. An RNA-sequencing transcriptome  
827 and splicing database of glia, neurons, and vascular cells of the cerebral cortex. *J.*  
828 *Neurosci.* 34, 11929–11947. <https://doi.org/10.1523/JNEUROSCI.1860-14.2014>

829

## 830 **Materials and Methods**

### 831 *Zebrafish husbandry*

832 All zebrafish lines were housed on a 14hr:10hr light:dark schedule in dechlorinated water at  
833 27.5°C and routine husbandry was performed by the UCL Zebrafish Facility. Embryos were  
834 collected from spontaneous spawning and staged according to Kimmel et al. 1995.

835 Embryos and larvae were raised on a 14hr:10hr light:dark schedule in 10cm Petri dishes at  
836 a density of 50 embryos per 10cm Petri dish. Embryo water (~pH7.3, temperature 28.5°C,  
837 conductivity ~423.7uS with methylene blue) was changed daily and animals over 4 days post  
838 fertilisation were euthanized by overdose of MS-222 (300 mg/l) or 15% 2-Phenoxyethanol  
839 (77699 SIGMA-ALDRICH) at the end of experiments.

840 Raising of genetically altered zebrafish and all experimental procedures were performed  
841 under project licence 70/7612 and PA8D4D0E5 awarded to JR under the UK Animals  
842 (Scientific Procedures) Act 1986 guidelines.

#### 843 *Lines*

Strain designation	Allele Number	Gene identifier	Additional Information
<i>10543/dmist<sup>vir</sup></i>	<i>la015577Tg</i>	ENSDARG00000095754	Maintained at UCL
<i>dmist<sup>i8</sup></i>	<i>u505</i>	ENSDARG00000095754	Maintained at UCL
<i>fxyd1<sup>Δ28</sup></i>	<i>u504</i>	ENSDARG00000099014	Maintained at UCL
<i>atp1a3a<sup>Δ19</sup></i>	<i>u513</i>	ENSDARG00000018259	Maintained at UCL
<i>atp1a3b<sup>Δ14</sup></i>	<i>u514</i>	ENSDARG00000104139	Maintained at UCL

844 Table 1. Zebrafish lines

845 The *dmist<sup>vir</sup>* allele was generated in wild type line T/AB-5 (Varshney et al., 2013) and  
846 outcrossed to Harvard AB. The *dmist<sup>i8</sup>*, *fxyd1<sup>Δ28</sup>*, *atp1a3a<sup>Δ19</sup>*, and *atp1a3b<sup>Δ14</sup>* alleles were  
847 generated and maintained at UCL on an AB/TL background. Both *dmist<sup>i8</sup>* and *dmist<sup>vir</sup>* were out-  
848 crossed to the AB strain at UCL for at least 3 generations.

#### 849 *Larval Zebrafish Behavioural Tracking*

850 At 4 days post fertilisation (dpf), zebrafish larvae were placed into individual wells of a 96-  
851 square well plate (WHA7701-1651 Sigma-Aldrich) filled with 650 µl of embryo water per well  
852 and tracked for 3 days under a 14:10 light:dark schedule (lights on-09:00, lights off-23:00) using  
853 automated videotracking in ViewPoint ZebraBoxes (Viewpoint Life Sciences). The 96-well plate  
854 was under constant illumination with infrared LEDs, and white LEDs simulated the light:dark  
855 schedule. Videography (with one-third inch Dragonfly2 PointGrey monochrome camera, frame

856 rate: 25-30 Hz; fixed-angle megapixel lens, Computar M5018-MP) of individual behavior was  
857 recorded in quantization mode to detect movement by background subtraction between frames  
858 in individual wells with 60 second integration time bins. Parameters used for detection were  
859 calibrated according to the sensitivity of individual boxes but were in the following range:  
860 detection threshold, 15-20; burst, 50 pixels; freeze, 3-4 pixels. Embryo water in the wells was  
861 topped up daily with fresh water, and ambient room temperature was maintained at  
862 approximately 26°C. Output data was sorted, parsed and analysed by custom Perl and Matlab  
863 scripts (MATLAB R2016 version 9.1, The MathWorks), as in Rihel et al. 2010.

864 Oxygen-permeable lids (Applied Biosystems 4311971) were applied over the top of the 96-  
865 well plate when performing experiments in constant darkness, and the larvae were left  
866 undisturbed for the duration of the experiment to avoid light exposure.

867 At the end of the experiment, all larvae were visually checked for health before euthanasia  
868 and transfer to individual wells of a 96-well PCR plate for DNA extraction and genotyping.

### 869 *Behavioural analysis*

870 Sleep parameters were calculated as in Rihel et al. 2010. For each genotype, exemplar  
871 experiments are shown, and summary data was analysed by combining experiments with a  
872 linear mixed effects model as follows. Behavioural summaries across multiple experiments  
873 were determined by using the Matlab fitlme function to fit a linear mixed effects model for each  
874 parameter with genotype as a fixed effect and independent experiment as a random effect,  
875 then representing the effect size as a % change from the wild type value. Before fitting the  
876 linear mixed effects model, the parameters sleep, sleep length, and waking activity were log  
877 normalized by calculating the log of 1+ the parameter value for each larva.

878 Circadian period for every larva was calculated using the Matlab findpeaks function on the  
879 activity (delta-pixels) timeseries data with a minimum peak distance of 18 hours (1080  
880 minutes). N-way ANOVA was calculated to evaluate differences between groups.

881 Code and data are available at <https://github.com/ilbarlow/Dmist>.

### 882 *Adult behavioural tracking*

883 Fish from a *dmist*<sup>#8/+</sup> x *dmist*<sup>#8/+</sup> cross were raised in a mixed gender tank to adulthood.  
884 Zebrafish adults (aged 3-4 months) were randomly selected and tracked on a 14:10 light:dark  
885 cycle (180 lux at water surface, lit from above) for three days as in (Chiu et al., 2016). In brief,  
886 fish were placed into uncovered plastic chambers (7x12x8.5 cm; WxLxH) with small holes for  
887 water exchange, and these were placed in a circulating water tank (46x54 cm with 4.5 cm water  
888 height). This setup was supplied with fish water from the home aquarium heated to 28°C and  
889 pumped from a 45 L reservoir at a flow rate of 1.3 L/min. Infrared light (60 degree, 54 LED  
890 Video Camera Red Infrared Illuminator Lamp, SourcingMap, with the ambient light detector  
891 covered) was continuously supplied from below. Fish were tracked at 15 Hz using Viewpoint  
892 Life Sciences ZebraBox tracking software in tracking mode, with a background threshold of 40,  
893 inactive cut-off of 1.3 cm/sec, and a small movement cut-off of 8 cm/sec. Each track was  
894 visually inspected for errors at one-minute resolution across the entire session and analysed  
895 using custom Matlab scripts (MATLAB R2016 version 9.1, The Mathworks, Inc). Experiments  
896 were performed blind to genotype, which was determined by fin-clip after the experiment.  
897 Females and males were originally analysed separately; since no significant gender effect was  
898 found (two-way ANOVA, genotypeXgender), data from both genders were pooled for the final  
899 analysis.

### 900 *Genotyping*

901 Prior to genotyping, adult fish were anaesthetised in 30 µg/ml MS-222, fin-clipped by cutting  
902 a small section of the caudal fin, and then allowed to recover in fresh fish water. For pooled



903 experiments, 3 dpf larvae from heterozygous in-crosses were fin-clipped as in Wilkinson et al.,  
904 2013 and allowed to recover in a square 96-well plate to keep larvae separate prior to pooling  
905 larvae of the same genotype. Genomic DNA was extracted from adult fin clips and larvae by  
906 boiling for 30 minutes in 50  $\mu$ l 1X base solution (0.025 M KOH, 0.2 mM EDTA). Once cooled,  
907 an equal volume (50  $\mu$ l) of neutralisation buffer (0.04 M Tris-HCl) was then added and undiluted  
908 genomic DNA used for genotyping.

909 The *dmist<sup>vir</sup>* genotype was detected by PCR (standard conditions) using a cocktail of three  
910 primers (0.36 mM final concentration each primer) to detect the wild type allele and viral  
911 insertion (see Table 2) so that genotypes could be assigned according to size of bands  
912 detected (*dmist<sup>vir/vir</sup>* 800 bp; *dmist<sup>vir/+</sup>* 508 bp and 800bp; *dmist<sup>+/+</sup>* 508 bp).

913 The *dmist<sup>#8</sup>* genotype was assigned by KASP genotyping using allele-specific primers  
914 (*dmist<sup>#8</sup>* allele 5'-GATCTCCCT[GCAGAAAGAT]CTTTCTGCA-3' = FAM, *dmist<sup>+</sup>* allele 5'-  
915 GATCTCCCT[CACCG]CTTTCTGCA-3' = HEX; KASP master mix KBS-1016-011) and assay  
916 were prepared and analysed according to manufacturer's protocol (LGC genomics).

917 The *atp1a3a<sup>A19</sup>* genotype was assigned by KASP genotyping using allele-specific primers  
918 (*atp1a3a<sup>A19</sup>* allele 5'-  
919 GACAGACTGAAGAAACAGCGACTGACGGCTC[CAAATGGGGTAAGAGTC]-3' = FAM,  
920 *atp1a3a<sup>+</sup>* allele 5'-GACAGACTGAAGAAACAGCGACTGACGGCTC-3'[] = HEX).

921 The *atp1a3b<sup>A14</sup>* genotype was assigned by PCR using MiSeq\_atp1a3b primers (Table 2),  
922 with the *atp1a3b<sup>A14</sup>* allele running 14 bp faster than the *atp1a3b<sup>+</sup>* allele.

923 *fxyd1<sup>A28</sup>* was assigned by KASP genotyping using allele-specific primers (*fxyd1<sup>A28</sup>* allele 5'-  
924 GAAGGTCGGAGTCAACGGATTTAATAAACTTTATTGTGCTTTTGTAGTTGT[A]-3' = HEX,  
925 *fxyd1<sup>+</sup>* allele 5'-  
926 GAAGGTGACCAAGTTCATGCTTAATAAACTTTATTGTGCTTTTGTAGTTGT[G]-3' = FAM)



927 or PCR using MiSeq\_fxyd1 primers (see Table 2) followed by digestion with the restriction  
928 enzyme DrdI, which yields bands at 138 bp and 133 bp for *fxyd1<sup>+/+</sup>*; 138 bp, 133 bp and 271  
929 bp for *fxyd1<sup>+/Δ28</sup>*, and 243 bp for *fxyd1<sup>Δ28</sup>*.

### 930 3'RACE

931 FirstChoice RLM-RACE kit (Ambion AM1700) was used to amplify the 5' and 3' ends from  
932 cDNA obtained from 4 dpf larvae raised on a 14:10 LD cycle and C57BL/6 E13.5 mouse  
933 embryos obtained from the Parnavalas lab (UCL). 5' and 3' RACE primers were designed  
934 according to the manufacturer's guidelines (Table 2) and the manufacturer's protocol was  
935 followed. Clones were sequenced by Sanger sequencing.

### 936 *In situ* hybridisation

937 Probes were designed to target the 3'UTR and entire open reading frame (ORF) of  
938 *dmist<sub>Dr</sub>* transcript using primers that amplified the target region from zebrafish cDNA under  
939 standard PCR conditions (expected size 1325 bp; Table 2). The PCR product was cloned  
940 into pSC vector (Strataclone PCR cloning kit Agilent 240205-12) and verified by Sanger  
941 sequencing. Antisense probe was generated by cleavage of pSC-dmist plasmid with XbaI  
942 and *in vitro* transcribed with T3 polymerase (Promega P2083) using 1 µg DNA template  
943 according to the standard *in vitro* transcription protocol (see the full protocol at  
944 [dx.doi.org/10.17504/protocols.io.ba4pigvn](https://doi.org/10.17504/protocols.io.ba4pigvn)). RNA probe was extracted and purified using the  
945 ZYMO RNA concentrator kit (Zymo #R1013).

946 Whole mount *in situ* hybridisation was performed according to (Thisse and Thisse, 2008)  
947 with the following adaptations. Embryos less than 5 dpf were dechorionated and fixed at the  
948 appropriate stage in 4% paraformaldehyde (PFA) overnight at 4°C. 5 dpf larvae were fixed in  
949 4% PFA/4% sucrose overnight at 4°C and then washed 3x5 min in PBS prior to dissecting out  
950 the brain. Fixed embryos were washed 3x5 min in PBS, progressively dehydrated into 100%  
951 methanol (MeOH) and stored at -20°C overnight. Prior to pre-hybridisation embryos were

952 bleached for 30 min in the dark (0.05% formamide, 0.5X SSC, 6% H<sub>2</sub>O<sub>2</sub>) and then fixed in 4%  
953 PFA for 30 min at room temperature. To image, the embryos were progressively rehydrated  
954 into 0.1% PBTw, progressively sunk in to 80% glycerol, and imaged on a Nikon compound  
955 microscope (Nikon Eclipse Ni, Leica MC190HD camera).

#### 956 *RT-qPCR*

957 Larvae from heterozygous in-crosses (*dmist<sup>i8/+</sup>* or *dmist<sup>vir/+</sup>*) were genotyped by tail biopsy at  
958 3 dpf (Wilkinson et al., 2013) and allowed to recover fully in individual wells of a square well  
959 96-well plate before euthanizing at 5 dpf. RNA was extracted from three 5 dpf embryos of each  
960 genotype by snap freezing in liquid nitrogen and TRIzol RNA extraction (Ambion 15596026)  
961 with the following modifications to the manufacturer's protocol: 400 µl total TRIzol reagent used  
962 to homogenise larvae using a pellet pestle homogenizer, and 5 µg glycogen (Invitrogen Cat  
963 No. 10814010; 20 µg/µl) was added to the RNA solution after chloroform extraction to aid  
964 precipitation of the RNA. The cDNA library was synthesised from high quality RNA (Agilent  
965 AffinityScript qPCR cDNA synthesis kit 600559), diluted 1:10, and gene-specific primers (Table  
966 2) were used for amplification of target genes with SYBR green mastermix in a BioRad CFX  
967 Real-Time qPCR instrument. Gene expression levels were normalised to the housekeeping  
968 gene *ef1alpha* (primers in Table 2) and analysed using custom Matlab scripts (MATLAB v9.2  
969 2017, The Mathworks 2017).

#### 970 *Sodium Green Assay*

971 Cell permanent Sodium Green tetraacetate (Invitrogen, S6901) was prepared fresh from  
972 frozen stock by dissolving in DMSO to 1 mM then diluting in fish water to a final concentration  
973 of 10 µM. About 50 larvae (5-7 dpf) from *atp1a3a<sup>Δ19/+</sup>* or *dmist<sup>i8/+</sup>* in-crosses were placed in  
974 wells of a 6 well plate, then most fish water was removed and replaced with 3 mL of the 10 µM  
975 Sodium Green solution for two hours. During exposure, the plate was covered in foil and placed  
976 in a 28°C incubator. For PTZ experiments, larvae were also exposed to 10 mM PTZ (diluted

977 from 1 mM stock dissolved in water) for two hours. For timepoints at night (ZT17-19), larvae  
978 were handled and collected under red light. After soaking in Sodium Green, larvae were  
979 washed 3X with fish water, anaesthetised with MS-222, and fixed in 4% PFA/4% sucrose  
980 overnight at 4°C. After 3X wash in PBS, larval brains were dissected and placed in 200 µL PBS  
981 in a 48 well plate, and the matched bodies were used for genotyping (see *Genotyping*). Brains  
982 were imaged using an upright MVX10 MacroView microscope with an MC PLAPO 1x objective  
983 (both OLYMPUS) with a mercury lamp for fluorescent excitation at 488 nm (OLYMPUS, U-  
984 HGLGPS). Images of roughly the same focal plane (dorsal/ventral view) were taken with an XM10  
985 OLYMPUS camera by a single exposure following minimal light exposure (to avoid bleaching).  
986 Mean fluorescent intensity was calculated from ROIs placed on the optic tectum/midbrain using  
987 ImageJ, background subtracted and normalized to the average fluorescence intensity for each  
988 imaging session.

### 989 *Protein Alignments*

990 Cross-species *dmist* homologues were identified by reciprocal BLASTp of the C-terminal  
991 region of *Dmist\_Dr* in vertebrate genomes. Translations of candidate transcript open reading  
992 frames were then aligned with *Dmist\_Dr* using ClustalOmega to calculate the percentage  
993 identity matrix ([www.ebi.ac.uk/Tools/msa/clustalo/](http://www.ebi.ac.uk/Tools/msa/clustalo/)) and visualised with the tool Multiple Align  
994 Show ([www.bioinformatics.org/sms/multi\\_align.html](http://www.bioinformatics.org/sms/multi_align.html)).

995 To identify *Dmist* orthologues, *Dmist* peptides were aligned with the multiple sequence  
996 alignment tool MAFFT (Kato and Toh, 2010) and seeded into a JackHMMR iterative search  
997 of the Uniprot database (Johnson et al., 2010). Protein-protein alignments of *Dmist* to *Fxyd1*  
998 were then performed using ClustalOmega and visualized with the tool Multiple Align Show.

### 999 *CRISPR/Cas9 gene targeting*

1000 CRISPR targets were designed and synthesised according to Gagnon et al., 2014 using  
1001 ChopChop (Montague et al. 2014; <http://chopchop.cbu.uib.no/>; see Table 2 for sequences) to

1002 identify target sites. 100 pg sgRNA and 300 pg Cas9 mRNA (pT3TS-nCas9n) were injected  
1003 into the yolk of 1-cell stage AB-TL embryos obtained from natural spawning. F0 fish were  
1004 screened by high resolution melt (HRM) analysis using gene-specific primers (Table 2) with  
1005 Precision melt supermix (Biorad 1725112) according to the manufacturer's protocol in a  
1006 BioRad CFX RT-PCR thermocycler. Positive founders identified in HRM analysis were then  
1007 sequenced by Illumina MiSeq using gene specific primers with adapters (Table 2) according to  
1008 the manufacturer's protocol.

### 1009 *Molecular cloning*

1010 GFP was fused to the *Dmist\_Dr* open reading frame (ORF) by Gateway cloning (Kwan et  
1011 al., 2007). Gene-specific primers were designed to amplify a PCR product that was recombined  
1012 with middle donor vector (Table 2; Invitrogen Gateway pDONR221 Cat No. 12536017,  
1013 Invitrogen Gateway BP Clonase II Cat No. 11789020) to generate a middle entry clone (pME-  
1014 *Dmist*). pME-*Dmist* was recombined with 5' (p5E-CMV/SP6) and 3' (p3E-GFPpA) entry clones  
1015 and destination vector (pDestTol2pA2) using Gateway Technology (Invitrogen LR Clonase II  
1016 Plus enzyme Cat No. 12538200) following the manufacturer's protocol.

1017 A 3 bp mutation was introduced into the *CMV:dreammist-GFPpA* by inverse PCR using  
1018 specific primers (Table 2) and KOD high fidelity hot start polymerase (Millipore 71085). The  
1019 template was degraded by DpnI digest and circular PCR product was transformed into  
1020 OneShot TOP10 chemically competent E coli (Invitrogen C4040). Both *CMV:dreammist-*  
1021 *GFPpA* and *CMV:dreammistA22W-GFPpA* constructs were checked by Sanger sequencing.

1022 For labelling the plasma membrane, mRNA was *in vitro* transcribed from pCS2-myr-Cherry  
1023 linearised with NotI, *in vitro* transcribed with SP6 mMessage mMachine (Ambion AM1340),  
1024 purified and quantified with a QuBit spectrophotometer, and injected at 0.04  $\mu\text{g}/\mu\text{L}$ .

### 1025 *Microinjection and imaging*

1026 For Dmist-GFP and DmistA22W-GFP live imaging, embryos from an AB-TL in-cross were  
1027 injected with 1 nL of plasmid (7 ng/ $\mu$ L). After developing to 90% epiboly, the embryos were  
1028 placed on a glass coverslip and observed on an inverted confocal microscope (SPinv, Leica)  
1029 with a 40X objective.

### 1030 *RNAseq*

1031 Larvae from heterozygous in-crosses ( $dmist^{i8/+}$  x  $dmist^{i8/+}$  and  $dmist^{vir/+}$  x  $dmist^{vir/+}$ ) were  
1032 raised to adulthood, genotyped and then homozygous mutant and wild type siblings were kept  
1033 separate. Homozygous mutant and wild-type sibling fish were then in-crossed so that first  
1034 cousins were directly compared. RNA was extracted from thirty 6 dpf larvae using the same  
1035 protocol as for RT-qPCR and sent for RNAseq analysis at the UCL Institute of Child Health  
1036 with a sequencing depth of 75 million reads per sample. Differential analysis of transcript count  
1037 level between groups was performed as in (Love et al., 2014), and additional analysis was  
1038 performed using custom Matlab scripts (MATLAB v9.2 2017, The Mathworks 2017).

### 1039 *Mouse RNAseq analysis*

1040 The dataset was downloaded from [https://web.stanford.edu/group/barres\\_lab/](https://web.stanford.edu/group/barres_lab/brain_rnaseq.html)  
1041 [brain\\_rnaseq.html](https://web.stanford.edu/group/barres_lab/brain_rnaseq.html); (Zhang et al., 2014) and hierarchical clustering (average linkage) and  
1042 Pearson correlation calculation analysis were performed using custom Matlab scripts  
1043 (MATLAB v9.2 2017, The Mathworks 2017).

### 1044 *Experimental Design and Statistical Analyses*

1045 Data was tested for normality using the Kolmogorov-Smirnov test. If data were normally  
1046 distributed, N-way ANOVA ( $\alpha=0.05$ ) was used with correction for multiple comparisons  
1047 using Tukey's test. If non-parametric, the Kruskal-Wallis test was used with correction for  
1048 multiple comparisons using Dunn-Sidak ( $\alpha=0.05$ ). Outliers were removed by Grubb's test  
1049 (threshold  $p<0.01$ ). P values from the linear mixed effects models were determined by are an  
1050 F-test on the fixed effects coefficients generated from the linear mixed effects model in Matlab.

1051 Data were grouped by genotype and gender for adult experiments and grouped by genotype  
1052 and day of experiment for larval experiments.

1053 All code is available at <https://github.com/ilbarlow/Dmist>.

1054

1055  
1056

**Table 2. Primer Sequences**

	Oligo Name	Sequence (5' -> 3')	Annealing temperature (oC)	Application
1	dmist_vir_fw	CACAGGGATGTGATGCCGGTTAAC	55	dmistvir genotyping
2	dmist_vir_rev	GTAGACACATACTGCCATACCAATC	55	dmistvir genotyping
3	vir_fw	CACCAGCTGAAGCCTATAGAGTACGAGC-	55	dmistvir genotyping
4	dmist_Dr_5RACE_fw	CGTTTCGCCACAATGTCAGCA	55-65	dmist_Dr 5'RACE
5	dmist_Dr_5RACE_rev_outer	AATGTTCAACTCCAGGCCGTC	55-65	dmist_Dr 5'RACE
6	dmist_Dr_5RACE_rev_inner	AATGTTCAACTCCAGGCCGTC	55-65	dmist_Dr 5'RACE
7	dmist_Dr_3RACE_fw_inner	GACGCCCTGGAGTTGAACATT	55-65	dmist_Dr 3'RACE
8	dmist_Dr_3RACE_fw_outer	GGTATGGCAGTATGTGTCTACA	55-65	dmist_Dr 3'RACE
9	Dmist_Mm_3RACE_outer	GCTGGTGA CTGCCTCCTTATG	55-65	dmist_Mm 3'RACE
10	Dmist_Mm_3RACE_inner	GTGTCTACAAGCCCATCCGTC	55-65	dmist_Mm 3'RACE
11	dmist_Dr_fw	TTTCGCCACAATGTCAGCAGC	56	dmist_Dr probe
12	dmist_Dr_rev	CGACTTTCATTTATTAGTTCAGACATGTC	56	dmist_Dr probe
13	qPCR_dmist_fw	ACGCCAGACCTTATGAAATCC	60	RT-qPCR
14	qPCR_dmist_rev	TGCGTCGGAGAGGTTTGATAG	60	RT-qPCR
15	qPCR_ankrd13a_fw	TGGTGGCGTTCCAGAGTTAC	60	RT-qPCR
16	qPCR_ankrd13a_rev	GGACACGAGAGGAATCCAGC	60	RT-qPCR
17	qPCR_slc6a4b_fw	ACATGGTTGGGTCGACGTTT	60	RT-qPCR
18	qPCR_slc6a4b_rev	TCCAACCCACCAAAAAGTGCT	60	RT-qPCR
19	ef1alpha_fw	TGCTGTCCGTGACATGAGGCAG	60	RT-qPCR
20	ef1alpha_rev	CCGCAACCTTTGGAACGGTGT	60	RT-qPCR
21	SP6dmist_sgRNA	ATTTAGGTGACACTATAGCGTTATGCAGAAAAGCGGTGGTTTTAGAGCTAGAAAATAGCAAG	n/a	CRISPR
22	T7atp1a3a_sgRNA	TAATACGACTCACTATAGACTGACGGCTCCAAAATGGGTTTTAGAGCTAGAAAATAGCAAG	n/a	CRISPR
23	SP6fxyd1_sgRNA	ATTTAGGTGACACTATAGGACCCCTCGCCAACACAAGGTTTTAGAGCTAGAAAATAGCAAG	n/a	CRISPR
24	SP6atp1a3b_sgRNA	ATTTAGGTGACACTATAGGACTGACTGCACAACCATGGTTTTAGAGCTAGAAAATAGCAAG	n/a	CRISPR
25	HRM_dmist_fw	GCCACAATGTCAGCAGCAGC	59	HRM
26	HRM_dmist_rev	GCGTTCACCTTAGACTCTCCCAGC	59	HRM
27	HRM_atp1a3a_fw	TGACAGACTGAAGAAACAGC	55	HRM
28	HRM_atp1a3a_rev	TTAAATCTCAGCACCAGCAG5	55	HRM
29	HRM_fxyd1_fw	TGACCAAACCTTCTTAAGGTGC	58	HRM
30	HRM_fxyd1_rev	AAATTGAGAAGACTTACTGGTCTGC	58	HRM
31	HRM_atp1a3b_fw	AAAGGCTGTCACCTTCTCCATCAC5	58	HRM
32	HRM_atp1a3b_rev	TGCAGTAGATGAGGAATCGGTC	58	HRM
33	MiSeq_dmist_fw	TCGTCGGCAGCGTCAGATGTGTATAAGAGACAGTATAACTTACGTGTGGACGGACTC	58	MiSeq
34	MiSeq_dmist_rev	GTCTCGTGGGCTCGGAGATGTGTATAAGAGACAGTTGCCTCAGCAGGATTTCCATAAG	58	MiSeq
35	MiSeq_atp1a3a_fw	TCGTCGGCAGCGTCAGATGTGTATAAGAGACAGTCGTTATCCGTGCAAGAGCTTC	58	MiSeq
36	MiSeq_atp1a3a_rev	GTCTCGTGGGCTCGGAGATGTGTATAAGAGACAGTCTCAGCACCAGCAGTTATCG	58	MiSeq
37	MiSeq_atp1a3b_fw	TCGTCGGCAGCGTCAGATGTGTATAAGAGACAGTACTGACATTCTCTCTTCGTG	68	MiSeq
38	MiSeq_atp1a3b_rev	GTCTCGTGGGCTCGGAGATGTGTATAAGAGACAGTTCTCTGTGATGCAGTAGATGAGG	68	MiSeq
39	MiSeq_fxyd1_fw	TCGTCGGCAGCGTCAGATGTGTATAAGAGACAGAAAATACTGTCTTGTGACCAAACC	57	MiSeq
40	MiSeq_fxyd1_rev	GTCTCGTGGGCTCGGAGATGTGTATAAGAGACAGTTCCATCTCTGCTGCAAAAATGC	57	MiSeq
41	attB1-dreammist forward primer	GGGGACAAGTTTGTACAAAAAAGCAGGCTTACCATGTCAGCAGCACGCCTGATCTCC	55-60	Gateway
42	attB3-dreammist reverse primer	GGGGACCACCTTTGTACAAGAAAGCTGGGTATCACCTGCGTGGAGAGGTTTGATAG	55-60	Gateway
43	Dmist-GFP A22Wfw	GCTTTCCAGTCTGGGAGTTGGCAGCTGGGAGAGTCTAAAG	66	SDM
44	Dmist-GFP A22WRev	CTTTAGACTCTCCAGCTGCCAACTCCAGACTGGAAAAGC	66	SDM



## 1057 **FIGURE LEGENDS**

### 1058 **Figure 1. A viral insertion mini-screen identifies a short-sleeping mutant, *dreammist*.**

1060 A-B) Mean  $\pm$  SEM sleep (A) and waking activity (B) of progeny from *dmist<sup>vir/+</sup>* in-cross from  
1061 original screen. White blocks show day (lights on) and grey blocks show night (lights off). Data  
1062 is combined from 2 independent experiments. n indicates the number of animals.

1063 C-F) Analysis of sleep/wake architecture for the data shown in (A, B). C) Quantification of total  
1064 sleep across two days and nights shows decreased day and night sleep in *dmist<sup>vir/vir</sup>*. Analysis  
1065 of sleep architecture reveals fewer sleep bouts during the day (D) and shorter sleep bouts at  
1066 night (E) in *dmist<sup>vir/vir</sup>* compared with sibling controls. F) Daytime waking activity is also  
1067 increased in *dmist<sup>vir/vir</sup>*. The black lines show the mean  $\pm$  SEM, except in E, which labels the  
1068 median  $\pm$  SEM. \*p<0.05, \*\*p<0.01, \*\*\*p<0.001; ns p>0.05; one-way ANOVA, Tukey's post hoc  
1069 test.

1070 G) Combining 5 independent experiments using a linear mixed effects model with genotype as  
1071 a fixed effect and experiment as a random effect reveals *dmist<sup>vir/vir</sup>* larvae have decreased total  
1072 sleep and changes to sleep architecture during both the day and night compared to *dmist<sup>+/+</sup>*  
1073 siblings. Plotted are the genotype effect sizes (95% confidence interval) for each parameter  
1074 relative to wild type. Shading indicates day (white) and night (grey). P-values are assigned by  
1075 an F-test on the fixed effects coefficients from the linear mixed effects model. \*p<0.05,  
1076 \*\*p<0.01, \*\*\*p<0.001, ns p>0.05. n indicates the number of animals.

1079 **Figure 2. *dmist* encodes a conserved vertebrate single pass transmembrane protein.**

1080 A) *dmist* mutants harbour a viral insertion in the 1<sup>st</sup> intron of *si:key-234h16.7*. *dmist* is syntenic

1081 with *Ankrd13* and *GIT* orthologs in mouse, human, and zebrafish.

1082 B) RT-qPCR of *dmist* (red) show reduced expression of *dmist* and not the 5' and 3' flanking

1083 zebrafish genes, *slc6a4b* (cyan) and *ankrd13a* (blue), in *dmist*<sup>vir/vir</sup> larvae compared to *dmist*<sup>vir/+</sup>

1084 and *dmist*<sup>+/+</sup> siblings. \*\*p<0.01, \*p<0.05; ns p>0.05; one-way ANOVA, Tukey's post-hoc test.

1085 Data shows mean ± SEM normalized to the wild type mean.

1086 C) *dmist\_Dr* contains an open reading frame encoding a 70 amino acid protein that is

1087 conserved across vertebrates. All identified homologues have a predicted signal peptide

1088 sequence (magenta line), signal peptide cleavage site (magenta circle), and predicted

1089 transmembrane domain (grey), with additional highly conserved C-terminal motifs (blue lines).

1090 Identical amino acids in all species are shown in black; similar amino acids (80-99% conserved

1091 across species) are shown in grey.

1092 D) *In situ* hybridisation using a *dmist* antisense probe reveals *dmist* is maternally deposited as

1093 it is detected at the 2-cell stage. At 24 hpf expression is restricted to regions containing

1094 neuronal precursors, and at 5 dpf expression is widespread throughout the brain. Tel,

1095 telencephalon; Dien, diencephalon; R1-6, rhombomeres 1-6; A, anterior; P, posterior. Scale

1096 bars= 0.5 mm (2 cell and 24 hpf), 0.1 mm (5 dpf).

1097 E-F) Representative confocal image of 90% epiboly embryo co-injected at the 1-cell stage with

1098 mRNA encoding membrane-RFP (magenta) and a plasmid encoding either C-terminal tagged

1099 Dmist-GFP (E, green) or DmistA22W-GFP (F, green). Scale bar= 25 µm.

1100

1101 **Figure 3. CRISPR-generated *dmist* mutants sleep less and are hyperactive at night.**

1102 A) CRISPR/Cas9 targeting of the first exon of *dmist* resulted in an 8 bp insertion (*dmist*<sup>#8</sup>) (grey

1103 line) within the coding sequence, leading to an early stop codon (red line with \*). Guide RNA

1104 target sequence and PAM sequence are shown as black bars. The sequence that is deleted in

1105 the mutant is indicated with a red bar.

1106 B) Predicted *Dmist*<sup>#8</sup> peptide sequence lacks most of the N-terminal signal peptide sequence

1107 (magenta) and the full C-terminus.

1108 C-D) Representative 48 hr traces of mean  $\pm$  SEM sleep (C) and waking activity (D) shows

1109 decreased sleep and increased waking activity at night for *dmist*<sup>#8/#8</sup> fish compared to *dmist*<sup>#8/+</sup>

1110 and *dmist*<sup>+/+</sup> siblings. n=number of fish.

1111 E-H) Analysis of sleep/wake architecture of the experiment depicted in (C, D) indicates that

1112 *dmist*<sup>#8/#8</sup> larvae sleep less at night (E) due to fewer sleep bouts (F). Sleep bout length is

1113 unchanged (G). Waking activity is also increased in *dmist*<sup>#8/#8</sup> fish (H). The black line represents

1114 the mean  $\pm$  SEM except for G, which is the median  $\pm$  SEM. \*p<0.05, \*\*p<0.01, \*\*\*p<0.001;

1115 One-way ANOVA, Tukey's post hoc test.

1116 I) Combining 5 independent experiments with a linear mixed effects model reveals *dmist*<sup>#8/#8</sup>

1117 fish sleep less at night due to fewer sleep bouts and also show increased waking activity at

1118 night. Plotted are the genotype effect sizes (95% confidence interval) for each parameter

1119 relative to wild type. Shading indicates day (white) and night (grey). P-values are assigned by

1120 an F-test on the fixed effects coefficients from the linear mixed effects model. \*p<0.05,

1121 \*\*p<0.01, \*\*\*p<0.001, ns p>0.05.

1122 J-K) (J) Adult *dmist*<sup>#8/#8</sup> fish have a higher mean swim speed compared to their wild type siblings

1123 at night. Data in (J) is quantified at night in (K). (J, K) show mean  $\pm$  SEM. \*p<0.05, one-way

1124 ANOVA.

1125 L) Cumulative probability distribution of all night-time swim bout speeds in adult fish. The  
1126 dashed lines show the half max (0.5 probability) for each curve. \* $p < 0.05$  for *dmist*<sup>#8/18</sup> fish  
1127 compared to wild type siblings; Kolmogorov-Smirnov test.

1128 **Figure 4. Mutation of the *dmist* related gene *fxyd1* causes reduced sleep at night.**

1129 A) Schematic of zebrafish Dmist and Fxyd1 protein domains and alignments comparing  
1130 human, mouse, and zebrafish Dmist and FXYD1 protein sequences. Black and grey shading  
1131 indicate amino acid identity and similarity, respectively. The FXYD domain is indicated with a  
1132 red line and the RRR motif in the C-terminus is indicated with a dark blue line.

1133 B) CRISPR-Cas9 targeting of the 3<sup>rd</sup> exon of *fxyd1* created a 28 bp deletion, resulting in a  
1134 predicted truncated protein. The start codon is marked by a cyan line. Guide RNA target  
1135 sequence and PAM sequence are shown as black bars. The mutant deleted sequence is  
1136 indicated with a red bar.

1137 C) *In situ* hybridisation of *fxyd1* at 24 hpf (whole animal) and 5 dpf brain (ventral view). Anterior  
1138 is to the left. Scale bar = 0.5 mm (24 hpf); 0.1 mm (5 dpf).

1139 D-E) Representative behavioral experiment showing *fxyd1*<sup>Δ28</sup> mutants have decreased night-  
1140 time sleep (D) but normal waking activity at night (E).

1141 F) Combining 5 independent experiments with a linear mixed effects model reveals *fxyd1*<sup>Δ28/</sup>  
1142 <sup>Δ28</sup> larvae sleep significantly less at night due to shorter sleep bouts compared to *fxyd1*<sup>+/+</sup>  
1143 siblings. Plotted are the genotype effect sizes (95% confidence interval) on each parameter  
1144 relative to wild type. Shading indicates day (white) and night (grey). P-values are assigned by  
1145 an F-test on the fixed effects coefficients from the linear mixed effects model. \* $p < 0.05$ ,  
1146 \*\* $p < 0.01$ , \*\*\* $p < 0.001$ , ns  $p > 0.05$ .

1147

1148 **Figure 5. Mutation of the Na<sup>+</sup>/K<sup>+</sup> pump alpha subunit *atp1a3a* reduces sleep at night**  
1149 A-B) Mean ± SEM sleep and waking activity traces of wild type larvae following exposure to 1  
1150 μM ouabain. Arrows indicate time the drug was added.  
1151 C-D) At night, sleep is significantly reduced and waking activity is significantly increased after  
1152 ouabain exposure. Student's t-test, one tailed.  
1153 E) Alignments of Na<sup>+</sup>/K<sup>+</sup> pump alpha subunits around the ouabain binding sites. Red indicates  
1154 residues that are critical for higher sensitivity to ouabain, which are present in mouse *Atp1a3*  
1155 but not *Atp1a1*.  
1156 F) *In situ* hybridisation of *atp1a3a* at 24hpf (whole animal) and 5dpf brain (ventral view).  
1157 Anterior is to the left. Scale bar = 0.5 mm (24 hpf); 0.1 mm (5 dpf). A-anterior; P-posterior; D-  
1158 Dorsal; V-Ventral  
1159 G) CRISPR-Cas9 targeting of the *atp1a3a* resulted in a 19 bp deletion that eliminates the start  
1160 codon (blue) and splice junction. Guide RNA target sequence and PAM sequence are shown  
1161 as black bars. Sequence that is deleted in the mutant is indicated with a red bar.  
1162 H-I) Representative behavioural experiment showing *atp1a3a*<sup>Δ19/Δ19</sup> fish are hyperactive  
1163 throughout the day-night cycle and have decreased sleep at night. Mean ± SEM are shown.  
1164 J) *atp1a3a*<sup>Δ19/Δ19</sup> larvae sleep less at night due to shorter sleep bouts. Plotted are the genotype  
1165 effect sizes (95% confidence interval) on each parameter relative to wild type. Shading  
1166 indicates day (white) and night (grey). P-values are assigned by an F-test on the fixed effects  
1167 coefficients from the linear mixed effects model. \*p<0.05, \*\*p<0.01, \*\*\*p<0.001, ns p>0.05.  
1168

1169 **Figure 6. *dmist* mutants have altered sodium homeostasis**

1170 A) Brain sodium levels are significantly elevated after exposure to PTZ in both *atp1a3a*<sup>Δ19/Δ19</sup>  
1171 (2 independent experiments) and *dmist*<sup>i8/i8</sup> (4 independent experiments) fish relative to wild  
1172 type and heterozygous mutant siblings, as measured by fluorescence intensity of Sodium  
1173 Green, normalized to the sample mean intensity. Crosses show mean ± SEM. n indicated the  
1174 number of animals. Below are example images of brains stained with Sodium Green. \*p<0.05,  
1175 \*\*p<0.01, one-way ANOVA, Tukey's post hoc test.

1176 B) Under baseline conditions, brain sodium levels are significantly elevated in *dmist*<sup>i8/i8</sup> fish at  
1177 night but not during the day, as measured by fluorescence intensity with Sodium Green.  
1178 Crosses show mean ± SEM. \*p<0.05, \*\*p<0.01, one-way ANOVA, Tukey's post hoc test.

1179 C) *dmist*<sup>i8/i8</sup> larvae have increased rebound sleep compared to wild type siblings following  
1180 exposure to 5mM PTZ. Representative sleep traces of *dmist*<sup>+/+</sup> (no drug, water vehicle controls  
1181 in black; PTZ exposed in blue) and *dmist*<sup>i8/i8</sup> (no drug in purple; PTZ exposed in red) following  
1182 1 hr exposure to 5 mM PTZ (black bar) in the morning. Data are mean ± SEM. *dmist*<sup>i8/+</sup> animals  
1183 are not plotted for clarity but are included in panel D.

1184 D) Rebound sleep after exposure to 5 mM PTZ, calculated from the experiment in C. Each dot  
1185 represents a single fish, grey lines show mean ± SEM.

1186 E) Effect size of change in sleep after 1 hr treatment with 5 mM PTZ (and washout) compared  
1187 to vehicle treated controls (error bars show 95% confidence intervals). \*p<0.05, one-way  
1188 ANOVA, Tukey's post-hoc test.

1189 F) Effect sizes (and 95% confidence interval) relative to wild types (dotted line) on sleep at  
1190 night in larvae from *dmist*<sup>+/+</sup>; *atp1a3a*<sup>+/+</sup> in-crosses from 3 independent experiments. P-values  
1191 are assigned by an F-test on the fixed effects coefficients from the linear mixed effects model  
1192 relative to *dmist*<sup>+/+</sup>; *atp1a3a*<sup>+/+</sup> animals. For all sleep-wake parameters, see Figure S6. \*p<0.05,  
1193 \*\*p<0.01, \*\*\*p<0.0001, ns p>0.05.

1194 **Figure S1. A viral insertion screen for sleep-wake regulators**

1195 A) Schematic of screening strategy. Candidate genes were selected from a list of 904  
1196 mammalian genes encoding protein classes most often linked to behavioural regulation,  
1197 including 1) genes previously implicated in sleep and circadian rhythms; 2) G-protein coupled  
1198 receptors; 3) neuropeptide ligands; 4) channels; and 5) proteins involved in post-translational  
1199 regulation, such as de-ubiquitinating enzymes (Supplemental Data 1). tBLASTN of the human  
1200 protein sequences identified 1162 zebrafish orthologs (Zv6), of which 702 (60.4%) had viral  
1201 insertions mapped in the 'Zenemark' zebrafish viral insertion library (Varshney et al., 2013).  
1202 Sperm harbouring viral insertions in 26 loci were successfully used for *in vitro* fertilization and  
1203 propagated to the F3 generation for screening. F3 larvae from single family F2 in-crosses were  
1204 monitored on a 14hr:10hr light:dark cycle from 4-7 dpf using videography and genotyped at the  
1205 end of the experiment.

1206 B-C) Histogram of total daytime sleep (B) and average daytime waking activity (C) normalized  
1207 as standard deviations from the mean (Z-score) of all the viral-insertion lines tested (including  
1208 heterozygous *vir/+* and homozygous *vir/vir*). Line 10543 (renamed *dreammist*) exhibited  
1209 decreased daytime sleep and increased daytime waking activity.

1210



1211 **Figure S2. *dmist*<sup>vir/vir</sup> fish are hyperactive and have normal circadian rhythms.**

1212 A) Free-running circadian period length of the locomotor activity of larvae from a *dmist*<sup>vir/+</sup> in-

1213 cross following the transition at 5 dpf from a 14hr:10hr light:dark cycle to constant dark

1214 conditions. The data is quantified for 48 hours after the shift to darkness and shows no

1215 difference in period between *dmist*<sup>vir/vir</sup> larvae and their sibling controls. Data is from 3

1216 independent experiments.  $p > 0.05$ , one-way ANOVA, Tukey's post hoc test.

1217 B-C) Representative mean  $\pm$  SEM sleep (B) and waking activity (C) traces of animals used to

1218 calculate circadian period length in (A). Light and dark grey blocks show subjective day and

1219 night, respectively.

1220 D) RT-qPCR time-course before (light) and after (grey) transfer into constant dark

1221 demonstrates that *dmist* mRNA levels do not oscillate with a circadian period, unlike *per1*

1222 mRNA which does.  $n=3$  replicates per timepoint. Expression is normalized to circadian time 3.

1223 Data are mean  $\pm$  SEM.

1224

1225 **Figure S3. *dmist* is enriched in neurons and requires the signal peptide cleavage site for**  
1226 **membrane localisation.**

1227 A) Relative expression level of *dmist* transcript from RNA sequencing of 6 dpf *dmist<sup>vir/vir</sup>* and  
1228 *dmist<sup>+/+</sup>* siblings. Z-scores were calculated by subtracting mean expression and normalising by  
1229 the standard deviation across all expressed transcripts (27,243 transcripts). Data show mean  
1230  $\pm$  SEM from 3 independent biological replicates. \*\* $p < 0.01$  Student's t-test.

1231 B) 3' and 5' RACE identify a long (1100 bp) and short (215 bp) 3'UTR variant in *dmist<sub>Dr</sub>*, and  
1232 a long 3'UTR (1050 bp) in *Dmist<sub>Mm</sub>*. The purple arrow indicates the ISH probe used in Figure  
1233 2D.

1234 C) *dmist<sub>Dr</sub>* sense probe negative control at 24 hpf shows no detectable expression.

1235 D) Percentage identity matrix comparing *Dmist* homologues across 6 vertebrate species  
1236 (100%=magenta; >70%=purple; >50%=cyan; <50%=green).

1237 E) Hierarchical clustering of RNAseq dataset of 6 different cell types isolated from the  
1238 developing (E13.5) mouse brain (Zhang et al., 2014) and post-hoc identification of *Dmist<sub>Mm</sub>*.  
1239 Data was standardized by subtracting the mean expression and normalizing by the standard  
1240 deviation across all expressed transcripts in each cell type (column). *Dmist<sub>Mm</sub>* (green arrow)  
1241 co-clusters with genes highly expressed in neurons (green shaded branches).

1242 F) Pearson rank correlation of canonical cell-type markers with *Dmist<sub>Mm</sub>* shows high co-  
1243 expression with neuronal markers compared to astroglial and endothelial cell markers. Data  
1244 are mean  $\pm$  SEM. \* $p < 0.05$ , \*\* $p < 0.01$ ; Kruskal-Wallis, Dunn-Sidak post-hoc test.

1245 G-I) Predicted processing of *Dmist* to its mature form in the plasma membrane (G). C-terminal  
1246 GFP fusion to *Dmist* is predicted to localise to the membrane (H). However, a mutation (A22W)  
1247 at the signal peptide cleavage site (I) is predicted to inhibit signal peptide cleavage and so  
1248 prevent proper subcellular localisation of the mature protein.

1249 **Figure S4. CRISPR-generated *dmist* mutants have reduced *dmist* transcript levels**

1250 A) RT-qPCR shows *dmist*<sup>#8/i8</sup> larvae have reduced *dmist* mRNA levels, suggesting that *dmist*<sup>#8</sup>  
1251 transcripts undergo nonsense mediated decay. Data are mean ± SEM of three biological  
1252 replicates. \*\*p<0.01; one-way ANOVA, Tukey's post-hoc test.

1253 B) Relative expression level of *dmist* transcript from RNA sequencing of 6 dpf *dmist*<sup>#8/i8</sup> and  
1254 *dmist*<sup>+/+</sup> siblings. Z-score calculated by subtracting mean expression and normalising by the  
1255 standard deviation across all expressed transcripts. Data are mean ± SEM for 3 independent  
1256 biological replicates. \*\*p<0.01, Student's t-test.

1257

1258

1259 **Figure S5. Ouabain dose curve and effects of *atp1a3b* mutation on behaviour.**

1260 A) Dose response curve of ouabain's effects on sleep at night, shown as mean  $\pm$  SEM and  
1261 normalized to the DMSO control. Each data point represents a single fish.

1262 B) Pearson rank correlation of canonical cell-type markers with *Atp1a3a\_Mm* shows high co-  
1263 expression with neuronal markers compared to astroglial and endothelial cell markers. Data  
1264 are mean  $\pm$  SEM.

1265 C) *In situ* hybridisation of *atp1a3a* at 24 hpf (whole animal) and 5 dpf brain (ventral view).  
1266 Anterior is to the left. Scale bar = 0.5 mm (24 hpf); 0.1 mm (5 dpf).

1267 D) CRISPR-Cas9 targeting of *atp1a3b* resulted in a 14 bp deletion that eliminates the start  
1268 codon (blue). Guide RNA target sequence and PAM sequence are shown as black bars. The  
1269 sequence that is deleted in the mutant is indicated with a red bar.

1270 E-F) Representative single behavioural experiment showing *atp1a3b* <sup>$\Delta$ 14/ $\Delta$ 14</sup> mutants have  
1271 increased daytime waking activity but normal sleep patterns.

1272 G) Data from 2 independent experiments combined with a linear mixed effects model. Plotted  
1273 are the genotype effect sizes (95% confidence interval) for each parameter relative to wild type  
1274 (dotted line) for each genotype. Shading indicates day (white) and night (grey). n indicates the  
1275 number of animals. P-values are assigned by an F-test on the fixed effects coefficients from  
1276 the linear mixed effects model relative to *atp1a3b*<sup>+/+</sup> animals. \*p<0.05.

1277

1278

1279 **Figure S6. Sleep effects in *dmist*<sup>-/-</sup>; *atp1a3a*<sup>-/-</sup> double mutants are non-additive.**  
1280 Combining 3 independent experiments with a linear mixed effects model reveals that the effects  
1281 of loss of function *dmist* and *atp1a3a* mutations are non-additive. Plotted are the genotype  
1282 effect sizes (95% confidence interval) for each parameter relative to wild type for each  
1283 genotype. Shading indicates day (white) and night (grey). n indicates the number of animals.  
1284

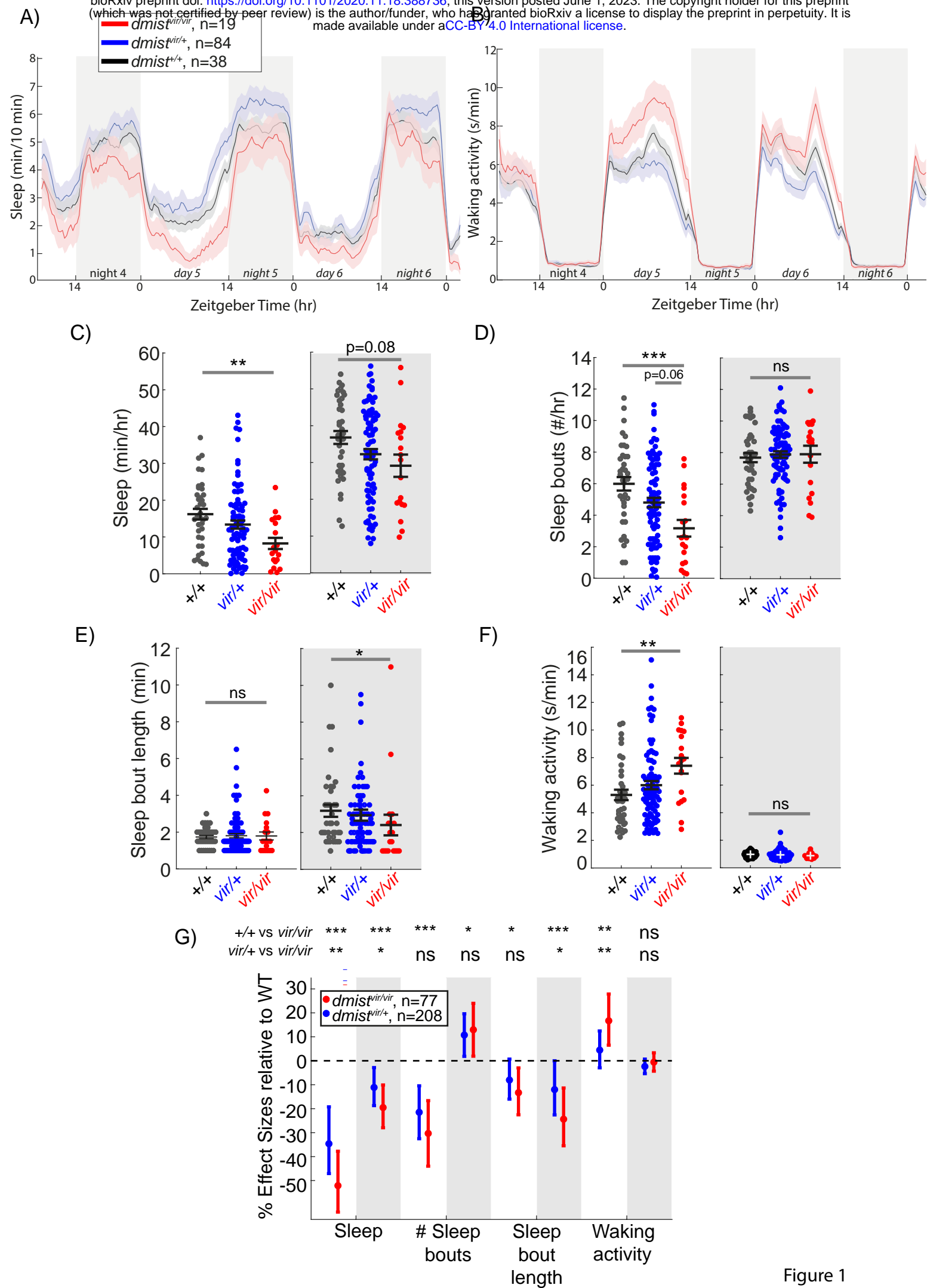


Figure 1

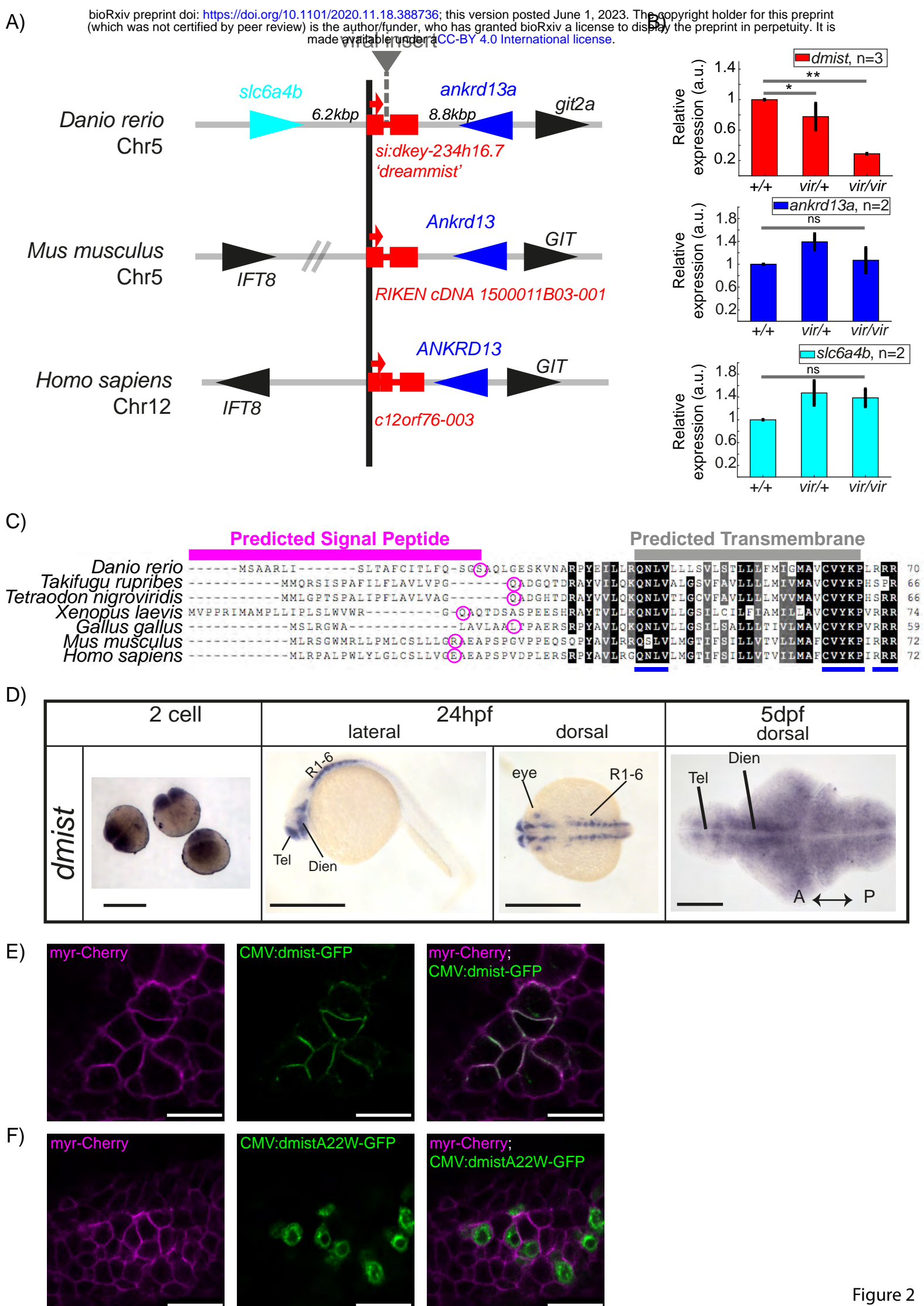


Figure 2



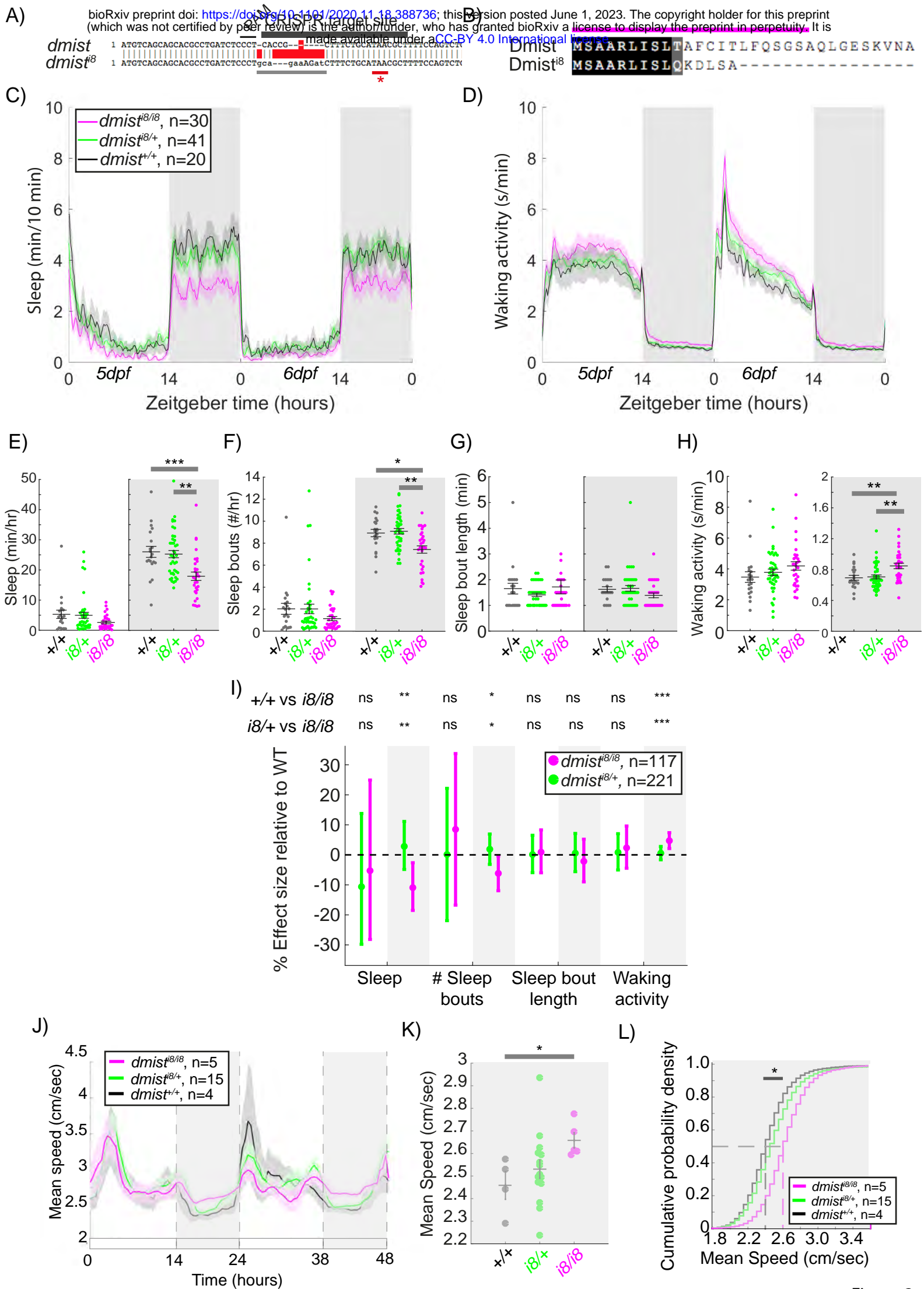


Figure 3

A)



DMIST\_Hs MLRPFALPWLWYLGICSL--VGEAEAPSPVDPLERSRPYAVLRGQNLVLMGTTFSSILLVTVILMA--FCVYKPI-----RRR 72  
 FXYD1\_Hs MASLGH---ILVFCVGLLTMAKAESPKEDDPFTYDYSLQIGGLVIAGILFILGLI--VLSRRRCCKFN--QQQRTGEPDEEEGTFRSSIRRLSTRRR 92

Dmist\_Mm MLRSQWMLLPMLCSLLLRGAEAPSPGVPPEQSQPYAVLRRQSLVLMGTTFSSILLVTVILMAF--CVYKPI-----RRR 72  
 Fxyd1\_Mm MASLGH---ILALCVCLLSMASAEAPQEPDPFTYDYHTLRIIGLTIAGILFILGLI--ILSKRCCKFN--QQQRTGEPDEEEGTFRSSIRRLSSRRR 92

Dmist\_Dr -MSAARLISLTAFCITLFQSGSAQLGESKVNARPYEILLR---QNLVL-LISVLSLTLILFMIGMAVCVYKPL-RRR-----70  
 Fxyd1\_Dr MMKSLALVFL-TFVPLVLAE-----GQQTTEDDPSFDYHRLRVGGLLILAAVLCILIGITILLSGHCRCKFNQDKRRRTGSNAQAMLNDTARASEC---89

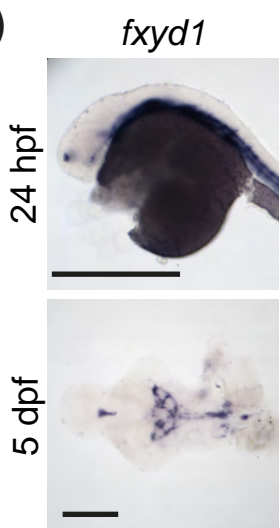
B)

*fxyd1*<sup>WT</sup> ATGATGAAATCTTTGGCACTAGTGTCTTGACATgtaagttgatttttttaataactgtctgtgacaaaacctcttaagtgctattttgataataaactttattgtgctttgttagTTGTGCCCTTGTGTTGGCAGAGGTCAT  
*fxyd1*<sup>Δ28</sup> ATGATGAAATCTTTGGCACTAGTGTCTTGACATgtaagttgatttttttaataactgtctgtgacaaaacctcttaagtgctattttgataataaactttattgtgctttgttagTTGT-----

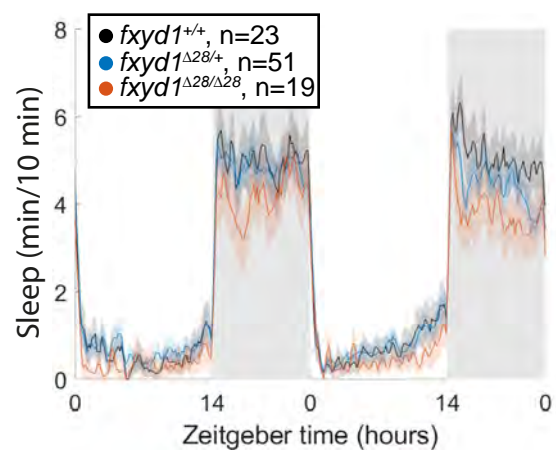
GCAGACCgtaagttctctcaattctttttattatgtgtagtgataaaaaagttaaataaaataaagtgttttttgccttgcatttgcagCAGAGGATGATCCCTTCTCTTTGtaagtttttttaaatatttaaat  
 ---ACCgtaagttctctcaattctttttattatgtgtagtgataaaaaagttaaataaaataaagtgttttttgccttgcatttgcagCAGAGGATGATCCCTTCTCTTTGtaagtttttttaaatatttaaat

Fxyd1<sup>WT</sup> MMKSLALVFLTFVPLVLAEGQQTTEDDPSFDYHRLRVGGLLILAAVLCILIGITILLSGHCRCKFNQDKRRRTGSNAQAMLNDTARASEC 89  
 Fxyd1<sup>Δ28</sup> MMKSLALVFLTFVPRQRMIPSLIITD----- 26

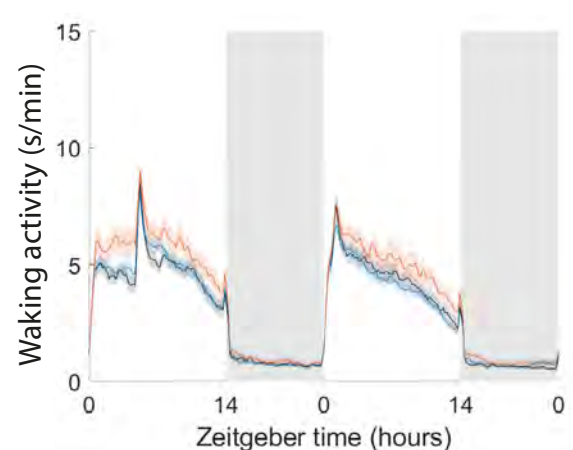
C)



D)



E)



F)

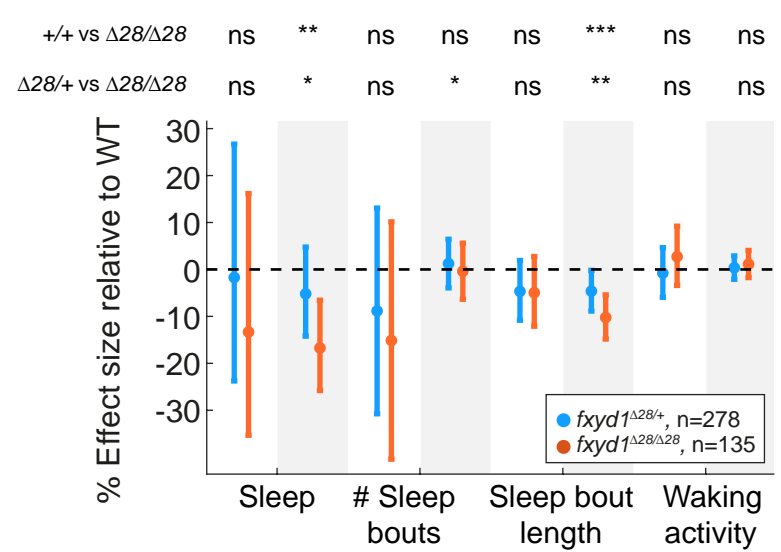


Figure 4

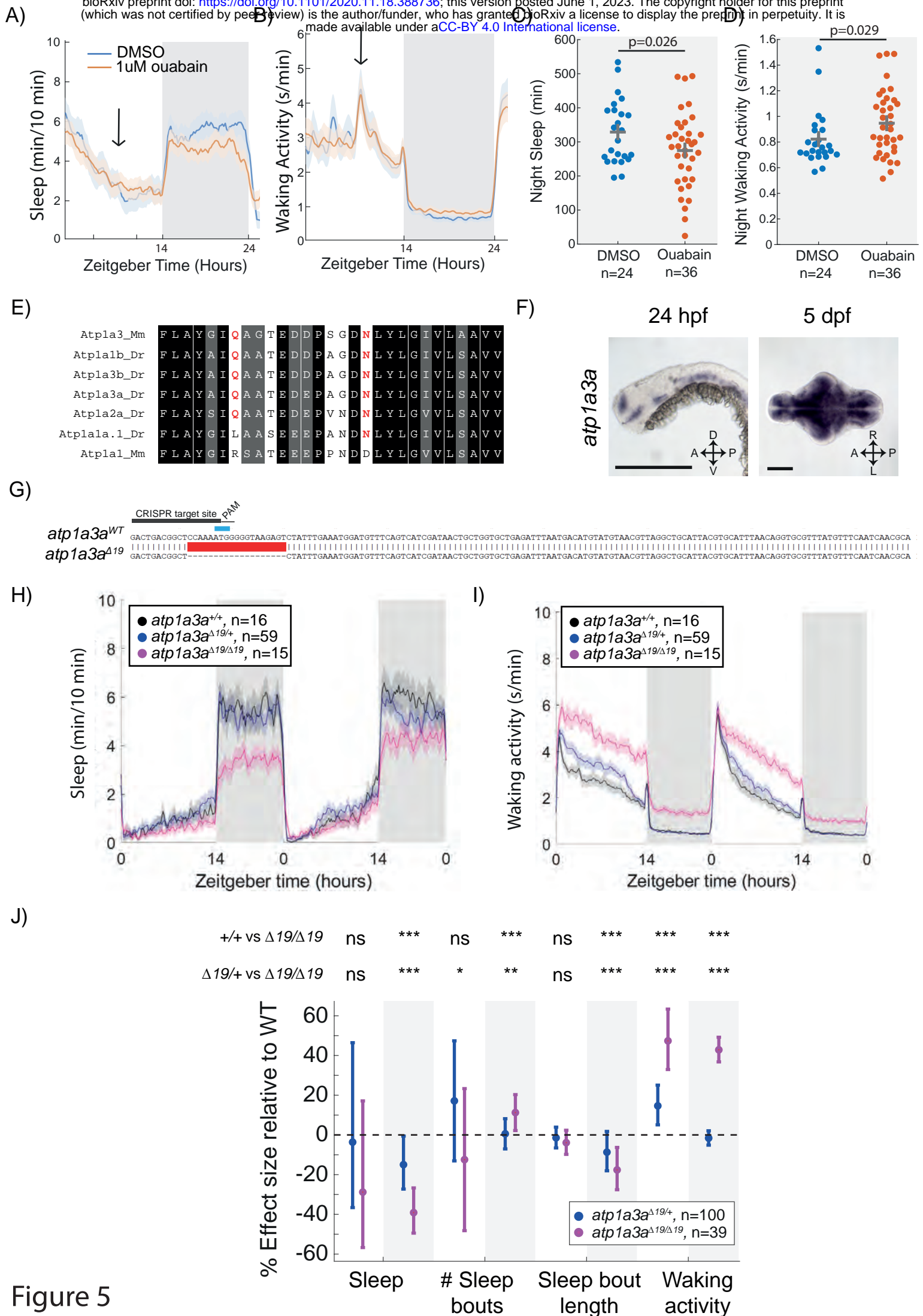


Figure 5

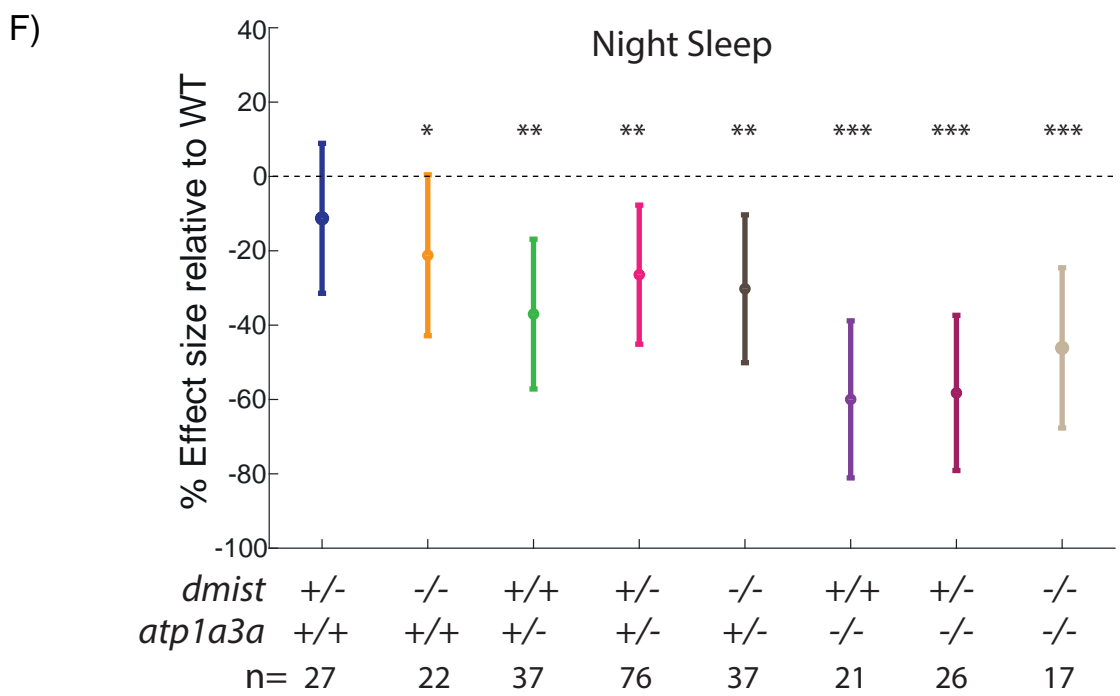
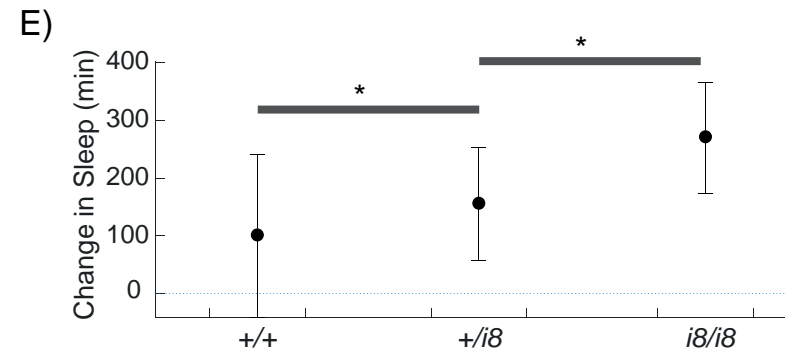
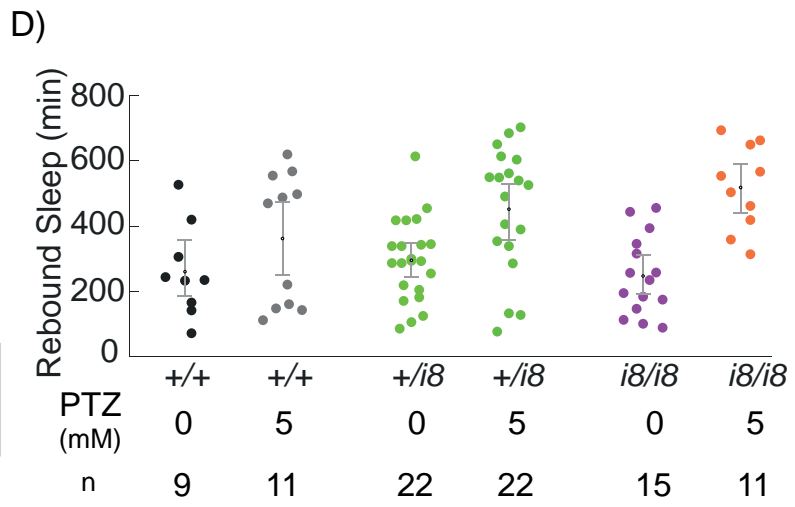
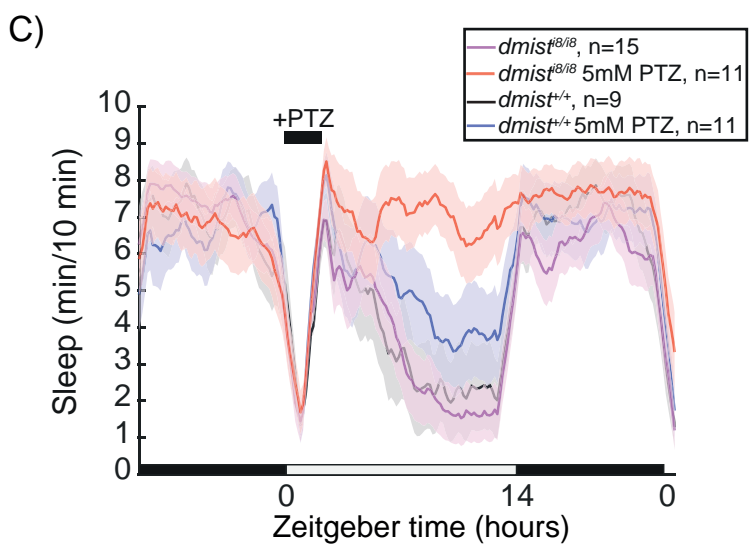
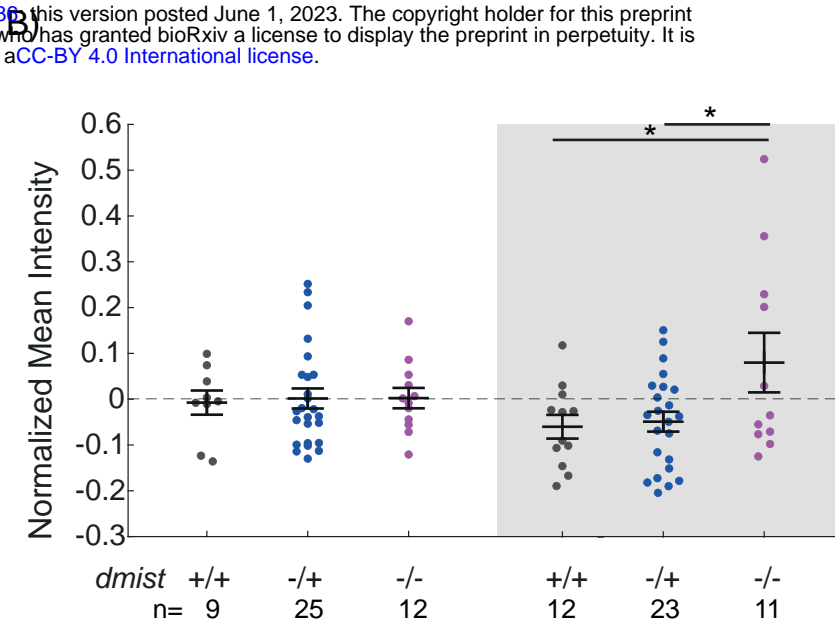
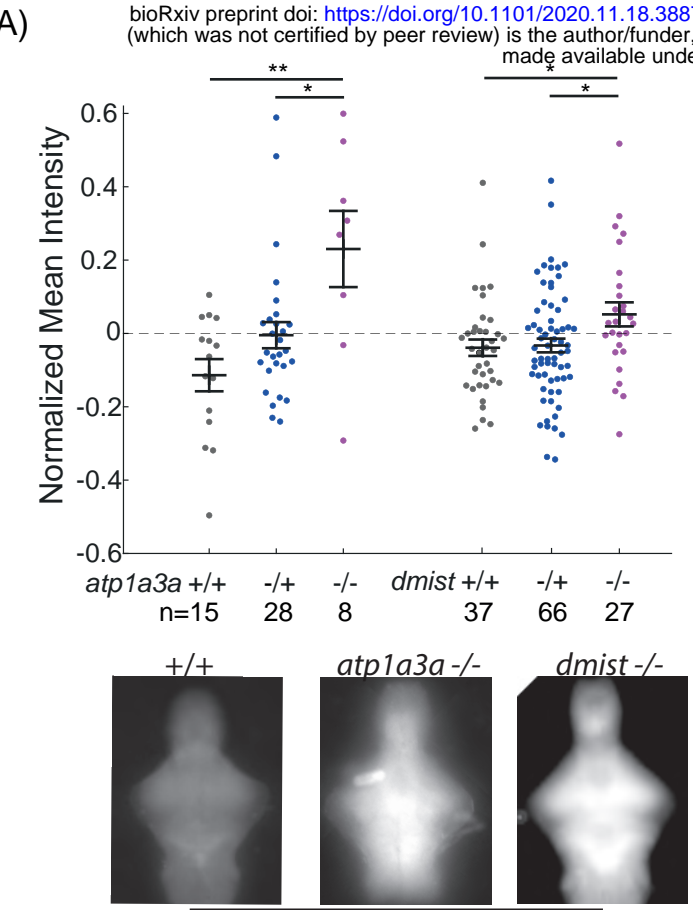
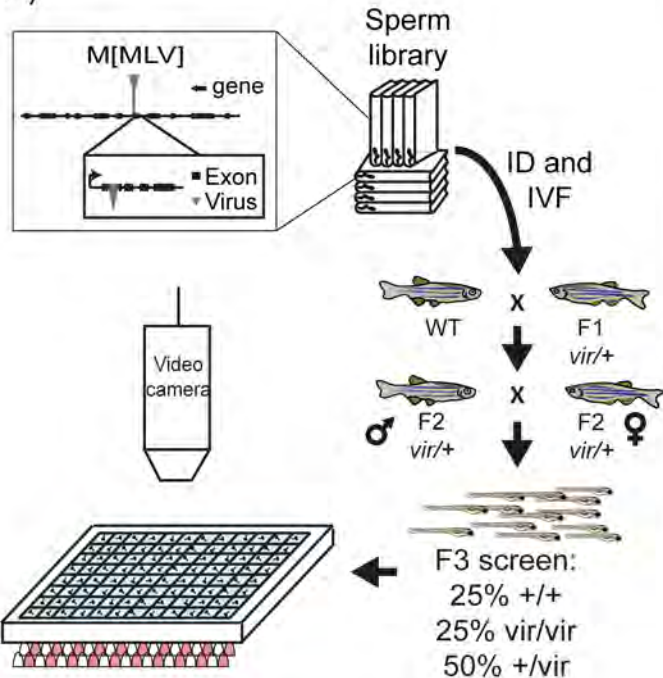


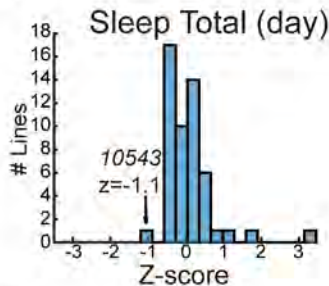
Figure 6

A)

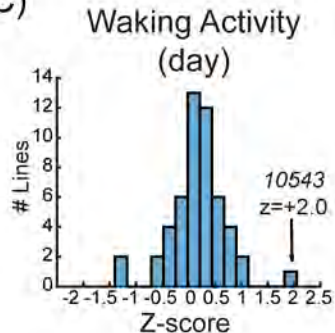


B)

Figure S1



C)





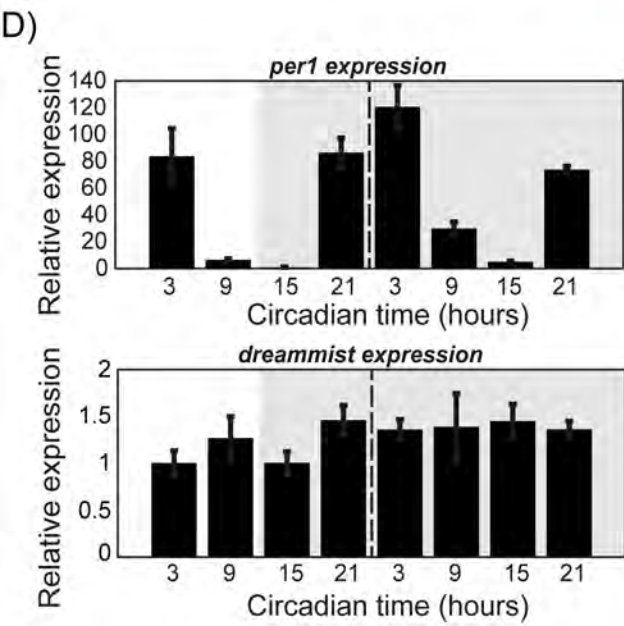
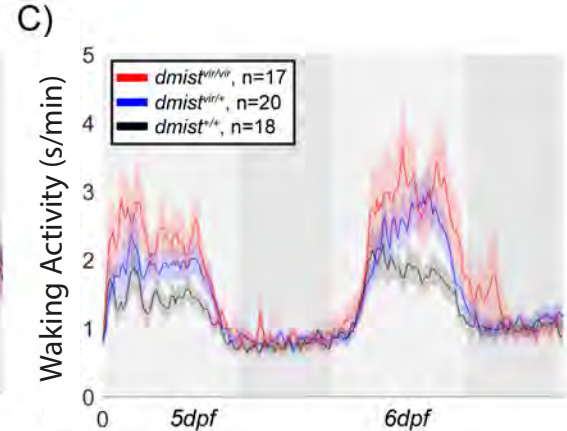
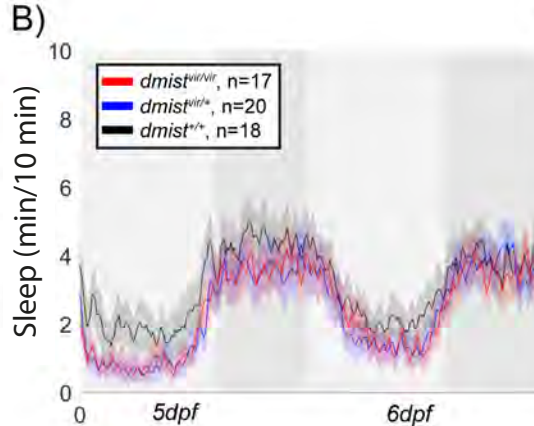
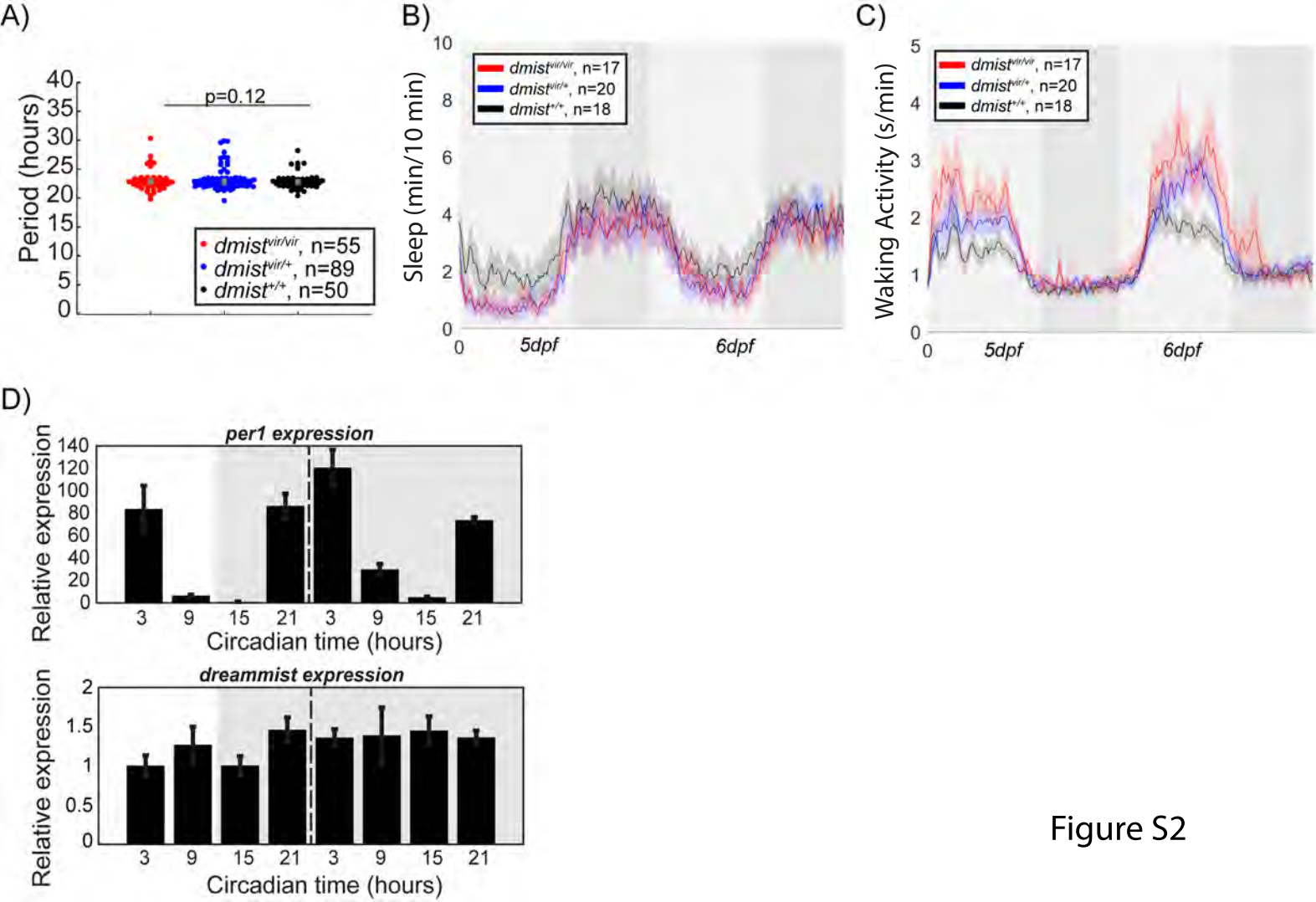
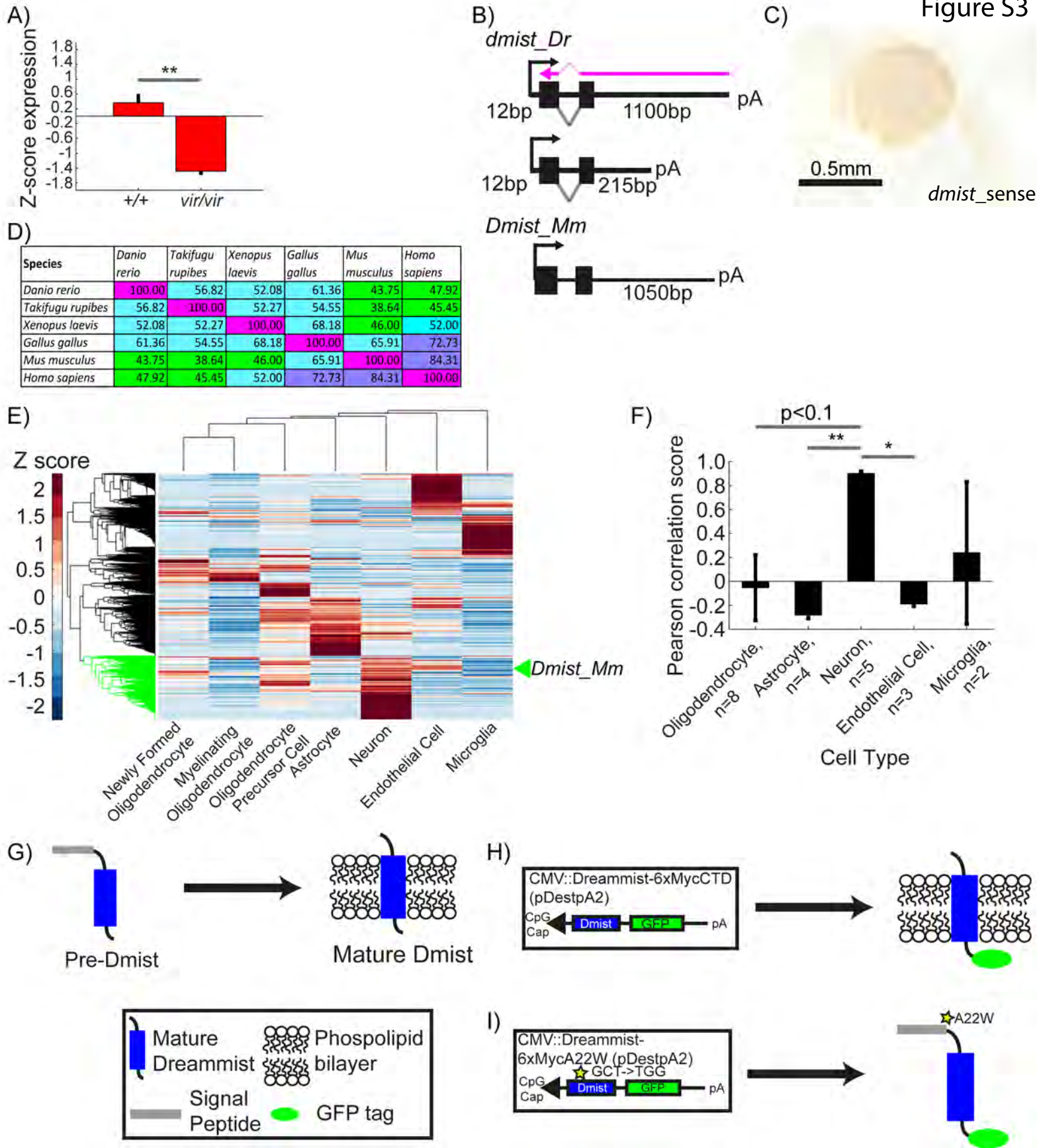


Figure S2





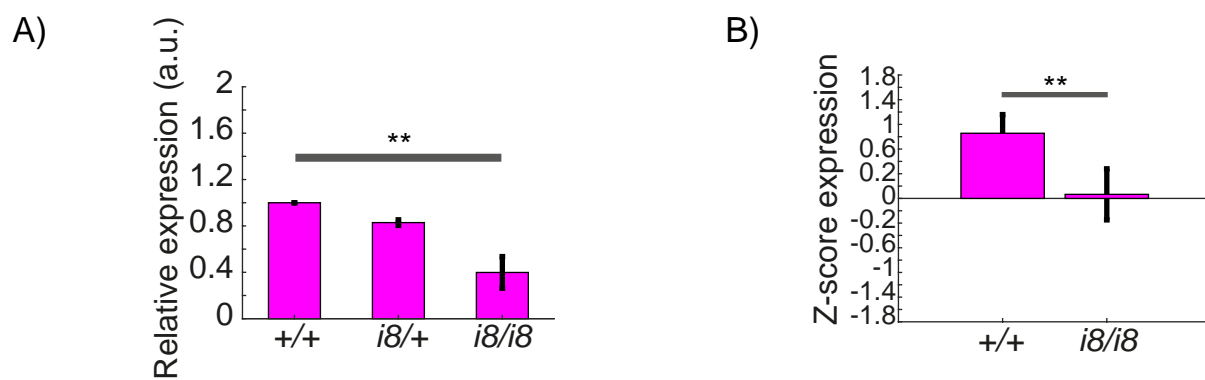


Figure S4

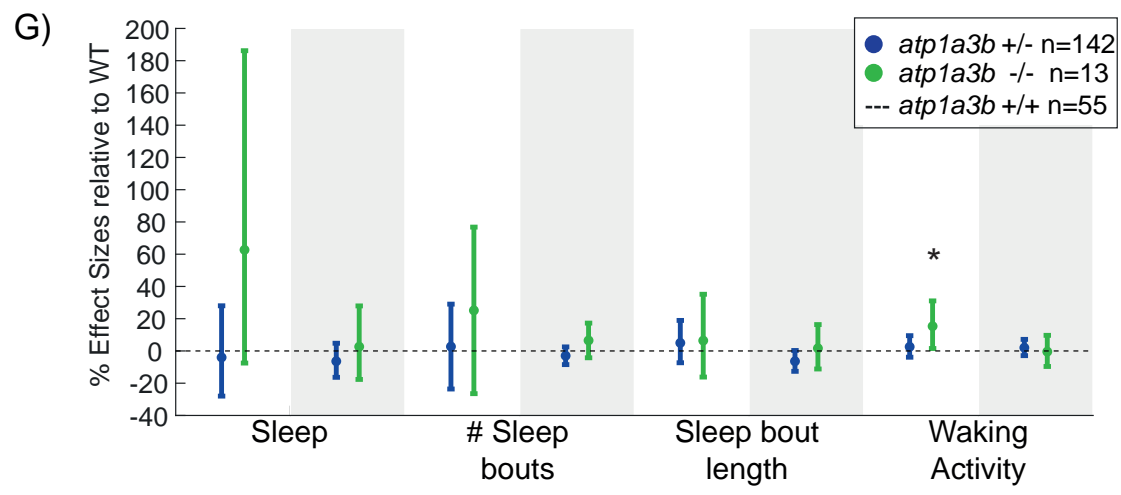
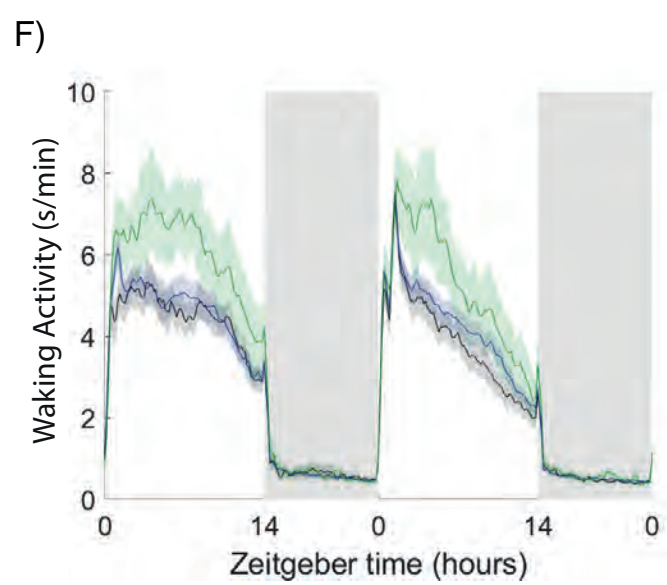
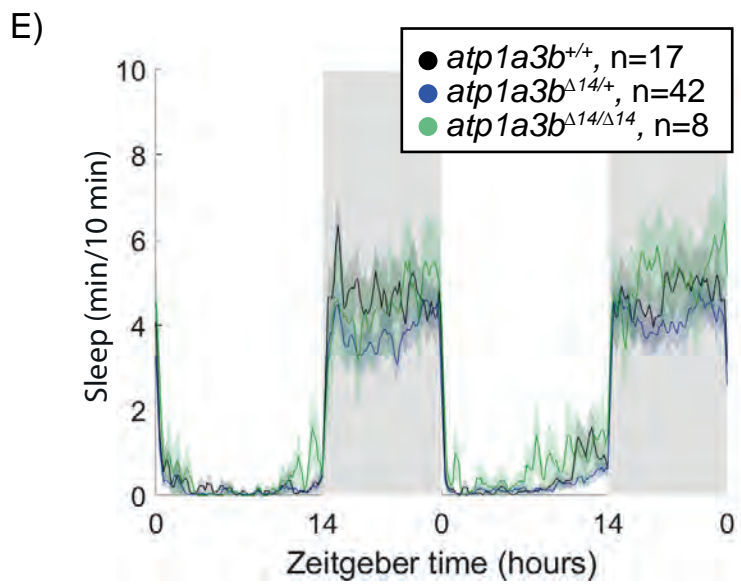
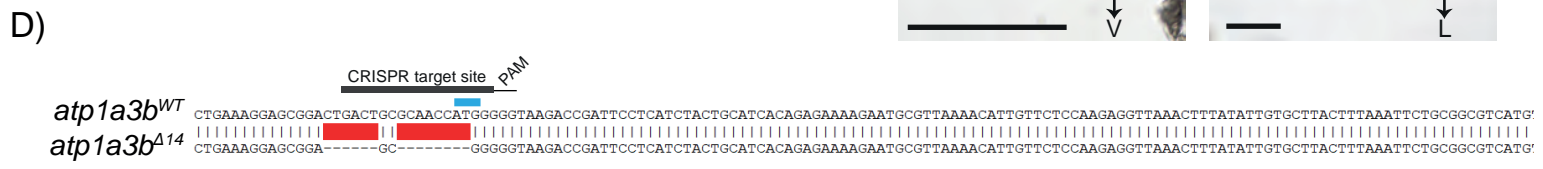
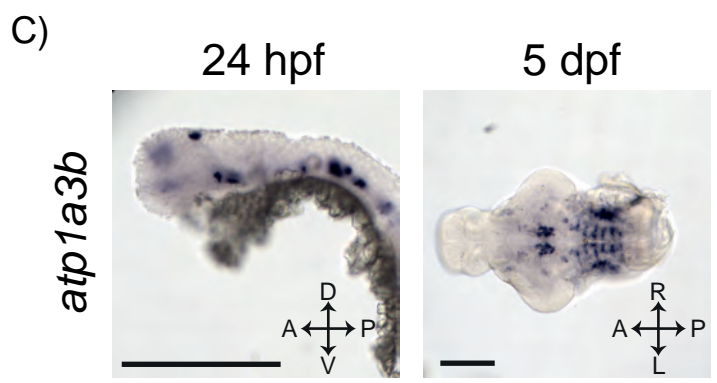
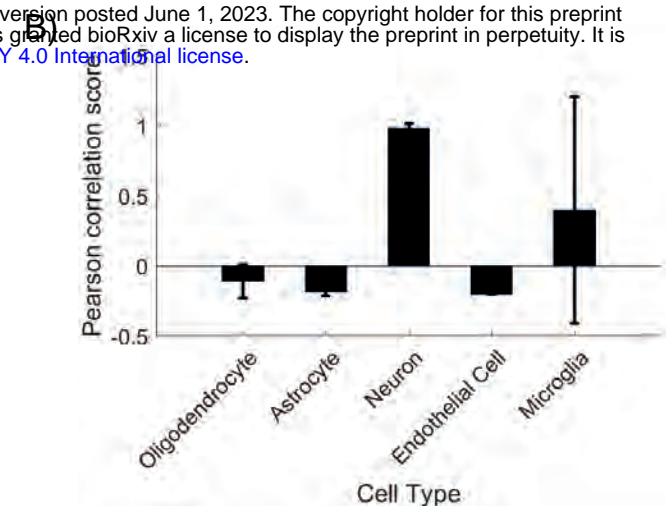
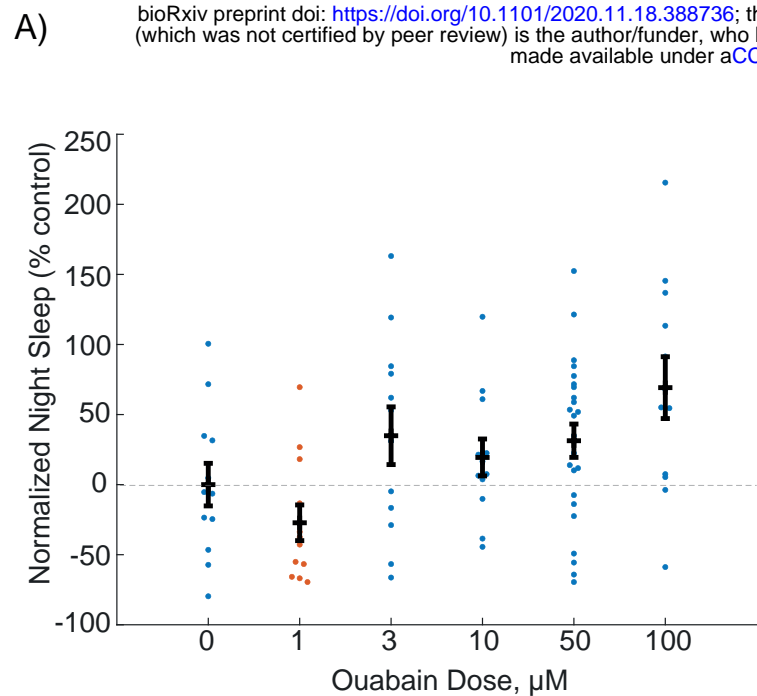


Figure S5

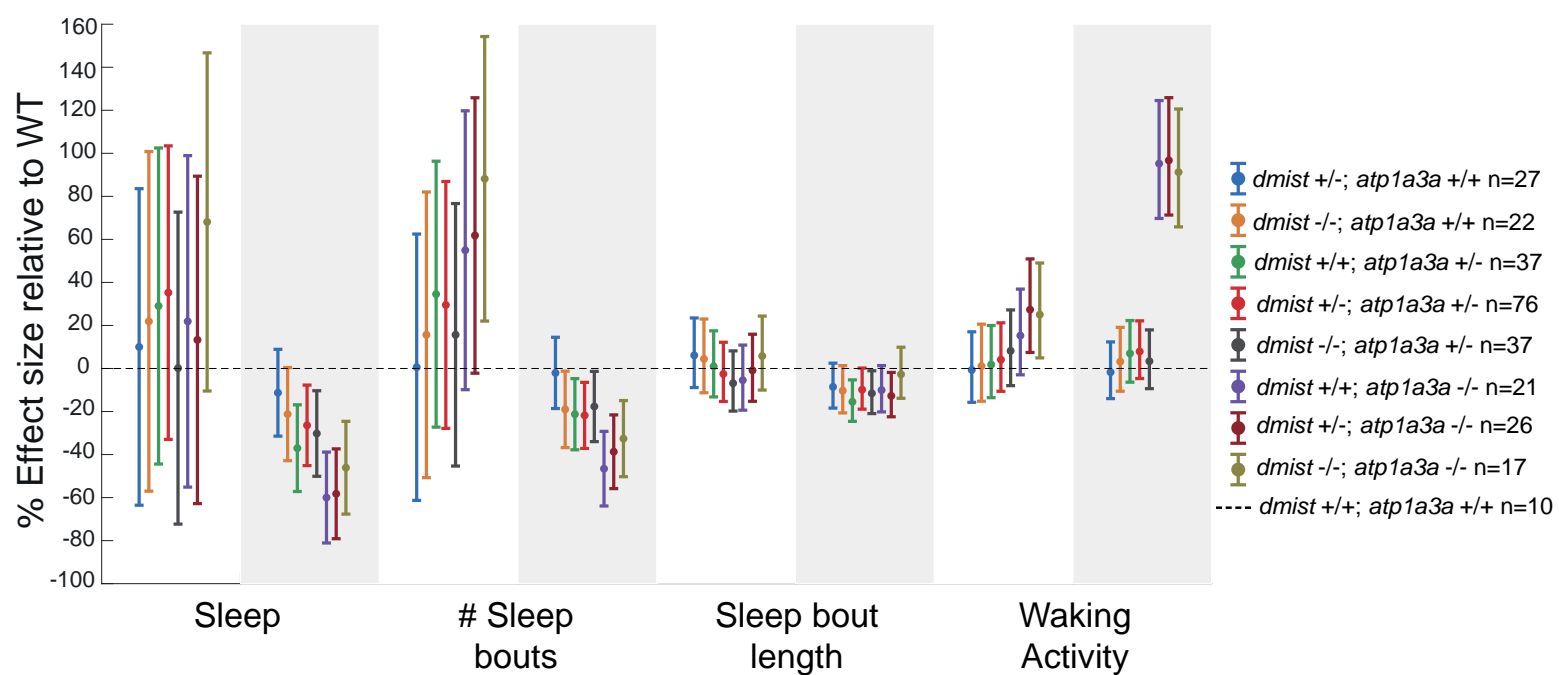


Figure S6